



Computational Investigation of the Phase Behavior of Colloidal Squares with Offset Magnetic Dipoles

Journal:	<i>Soft Matter</i>
Manuscript ID	SM-ART-01-2023-000081.R1
Article Type:	Paper
Date Submitted by the Author:	09-May-2023
Complete List of Authors:	Dorsey, Matthew; North Carolina State University at Raleigh, Chemical and Biomolecular Engineering Velev, Orlin; North Carolina State Univ., Chemical Biomolecular Engineering Hall, Carol; North Carolina State University, Chemical and Biomolecular Engineering

ARTICLE

Computational Investigation of the Phase Behavior of Colloidal Squares with Offset Magnetic Dipoles

Matthew A. Dorsey,^a Orlin D. Velev,^a and Carol K. Hall*^a

Received 00th January 20xx,
Accepted 00th January 20xx

DOI: 10.1039/x0xx00000x

Colloidal particles with anisotropic shapes and interactions display rich phase behavior and have potential as structural bases for materials with controllable properties. In this paper, we explore the self-assembling characteristics of a new class of particles that have been shown experimentally to form reconfigurable structures: microscopic cube-shaped colloids with a magnetic dipole that is transversely offset from the particle's center of mass. We have performed *in silico* simulations of the dynamics of large numbers of dipolar squares in two-dimensions using discontinuous molecular dynamics (DMD). We use a coarse-grain method where the dipolar microcubes are represented by a group of four hard circles bonded together to create a rigid square in two-dimensions and two opposite charges are embedded within the square to represent a magnetic dipole. Annealing, or "slow-cooling", simulations are conducted to determine the equilibrium structures. Systems of dipolar squares tend to assemble into one of two different types of conformations: either single- or double-stranded assemblies, each with unique structures and phase diagrams in the temperature-density plane. Single-stranded assemblies form highly interconnected percolated, or gel-like, networks. In contrast, double stranded assemblies tend to form globally-aligned nematic states at high densities, although this is not seen consistently in all runs. The phase behavior of systems of dipolar squares depends not only on the system's temperature and density, but also on the type of dipole embedded within the microcube and on the relative number of cubes with an opposite "handedness" that are present within the system.

Introduction

Colloidal self-assembly relies on interparticle forces to direct systems of particles into ordered structures. Colloidal assemblies can have many different morphologies, including lattices, strings, sheets, and vesicles (1). Often, they can be induced to reversibly switch between phases by adjusting the forces between the particles with specific external stimuli, e.g., electromagnetic fields (2). Colloidal systems with tailored properties that change predictably and reversibly in response to external stimuli are the basis for functional materials with tunable and controllable properties. Applications for these materials are increasingly being found in areas like biotechnology (3–5), photonics (6–9), and electronics (10–12). For example, dense suspensions of colloidal spheres self-assemble into 2D monolayers and 3D multilayers with controllable lattice properties, which then act as templates for optical etching masks in photolithography (13).

Colloidal particles with anisotropic properties are of interest because they exhibit phase behavior that is more complex than their isotropic analogs (14). One prominent example of an anisotropic colloid is Janus spheres, which are spherical colloids whose two hemispheres have different physical or chemical properties (15). As a result of their different properties, Janus spheres have interactions that depend on their relative orientation. Spherical colloids with isotropic interactions

assemble into symmetrical, lattice-like configurations at high densities (e.g. face-centered cubic, hexagonal close-packed, and body-centered cubic lattice structures). The packing structure of systems with hard shapes is entropically driven: the system's overall free-energy is minimized at high densities when colloidal particles organize into structures with fewer configurational possibilities (16). However, Janus particles, whose interaction symmetry has been broken, assemble into a rich variety of phases distinct from their isotropic analogs. Amphiphilic Janus particles, whose hemisphere's have different physical properties (e.g. hydrophilic and hydrophobic) have surfactant-like behavior, assembling into micelle and bilayer phases (17,18). Colloids with internal dipoles also have orientationally-dependent interactions (19–21). Janus spheres with an internal, centrally-located magnetic or electric dipole form into staggered chains and branched structures at low densities, and into crystal structures at high densities (22–24). The geometry of a colloidal particle also plays an important role in a system's phase behavior, especially at high densities. For example, colloidal rods at high densities order into smectic and nematic phases in which all particles are globally oriented in the direction of their long axis (25).

In this paper we explore the behavior of cube-shaped colloidal particles that have an internal magnetic dipole and which have been confined to a 2D plane. The focus is on a novel class of cubic, metallodielectric microparticles introduced by Han et al. that are able to interact, assemble, reconfigure, and propel in response to external magnetic and electric fields (26–28). These "patchy" cubic microparticles are 10 μm in size and

^a Department of Chemical and Biomolecular Engineering, North Carolina State University, Raleigh, NC 27606. Email: hall@ncsu.edu

are generated by coating one face of a cubic latex particle with a thin layer of cobalt, a ferrometallic material. When the particles are suspended in solution, they sediment to the bottom of the thin chamber, effectively reducing the geometry to two dimensions. Application of an external magnetic field across the chamber parallel to the floor causes the metallic coating to acquire residual magnetic polarization that creates long-range, directionally-dependent forces between the patchy microparticles. The magnetic field also forces the particles to orient their magnetic side along the direction of the magnetic field, leading to the formation of chained assemblies. The combination of particle geometry, directional dipole-dipole interparticle magnetic interactions, and responsiveness to externally-applied, tunable and time-dependent magnetic and electric fields gives these particles a rich potential for assembling into responsive and reconfigurable materials.

Computer simulations have been used extensively to study the effect that particle geometry and orientationally-dependent interactions (e.g., dipole-dipole interactions) have on the self-assembling behavior of anisotropic colloidal particles (29–32). Molecular dynamics simulations are often used to model the motion of colloidal suspensions by approximating forces between particles with pairwise interparticle potential functions (33–35). Computational studies of circular colloids with offset internal dipoles have predicted a range of phase behavior depending on the location and orientation of the dipole embedded in the particle (36). In previous studies, computer simulations have also been used to study systems of colloidal cubes with internal dipoles (37–41). One challenge with the modeling of systems of non-spherical colloids is in properly accounting for their excluded volume interactions. Due to their anisotropic geometries, computer simulations must account for both the translational motion and the rotational motion of the particle, increasing their overall computational burden. To alleviate this burden, colloids with anisotropic geometries are often approximated as groupings of particles with isotropic interactions. For example, Escobedo et al. performed Monte Carlo simulations of hard geometries in two- and three-dimensions, modelling the squares and cubes, respectively, as clusters of hard-spheres (42,43). The same method was used by Kantorovich et al. to study cubes with embedded, centrally-located magnetic dipoles, in which the magnetic dipoles were represented by the point charge-dipole equation (44,45). While theoretical studies of spheres with offset dipoles and of squares with centrally-located dipoles have been performed extensively using a variety of models, computational simulations of squares with offset dipoles have not yet been performed to the best of our knowledge. Colloids with offset dipoles can be grouped into two categories depending on how the dipole is shifted from the particle's center-of-mass. If the vector that points from the particle's center of mass to the center of the offset dipole is parallel to the direction that the dipole points, the dipoles are considered longitudinally shifted. If that same vector points perpendicular to the direction that the dipole points, the dipoles are considered transversely shifted.

The goal of this work is to explore the phase behavior of the polarized square colloidal particles with transversely-shifted internal magnetic dipoles introduced by Han et al (26). We model square colloidal particles in 2D as a cluster of four hard, non-overlapping circles that are bonded together to create a rigid, square geometrical shape in two dimensions. We model the square's dipole as two opposite charges embedded within the hard spheres on the square's edge, so that the dipole points parallel to one of the principle axes of the square. The interaction between two charges is defined such that charges with the same sign experience a repulsive potential, while charges with opposite signs experience an attractive potential. This construct is analogous to an electrostatic dipole, and has been used previously to model magnetically-polarized colloids (46–48). One unique feature of the magnetically-polarized colloids is their chirality. Since the squares are unable to rotate outside of the two-dimensional simulation plane, they have a fixed chirality, which depends on the direction of their magnetic dipole relative to the square's center. Another unique feature of these magnetically-polarized colloids is that their dipole is offset from the particle's center. Here we study two different types of dipoles, which we denote as standard and offset dipoles, and which differ in how the dipole is embedded within the square.

Highlights of our results include the following. We find that, for all systems, as the temperature is reduced below a threshold value, the dipolar square particles assemble into one of two types of structures: 1) single-stranded assemblies, or 2) double-stranded assemblies. In a single-stranded assembly, the squares aggregate primarily in head-to-tail configurations, to form flexible assemblies in which all the dipoles in the strand point in the same direction. In a double-stranded assembly, pairs of dipolar squares in an anti-parallel conformation aggregate to form rigid assemblies with rod-like morphologies. We have found that the system's preference for assembling into either single-stranded or double-stranded assemblies is a consequence of where the dipole is embedded within the square, which affects the squares' preference for either head-to-tail or antiparallel configurations. Additionally, we find that under certain conditions, systems of magnetically polarized squares with transversely shifted dipoles exhibit density-dependent percolation and nematic phase transitions. Interestingly, these phases depend not only on the type of dipole embedded within the square, but also on the presence or absence of squares of opposite chirality in the system.

Model

The square particle is modeled with four non-overlapping, uniform hard discs of diameter σ . The square geometry is maintained by bonding the hard discs in each group in such a way that the square maintains a rigid shape, as shown in Fig. 1. Five pseudo-bonds are used for each square via Bellemans' method (49). In Bellemans' method, spheres bound together experience a repulsive force if their distance from one another is outside of a certain range. Bellemans' constant, δ , defines how tightly the discs are bound to one another, which was set

to 0.015σ for our simulations. Two small, charged discs, opposite in "charge" but equal in magnitude, are embedded in the first and second discs of each square formation, shown in Fig. 2. In our model, squares are unable to rotate outside of the simulation plane, and, as a result, they have a fixed chirality over the course of any simulation (50). The chirality of any square depends on where the charges are embedded relative to the particles center. We define A-chirality squares to have a magnetic dipole that points clockwise relative to the center of the particle, and B-chirality squares to have a magnetic dipole that points counterclockwise relative to the center of the square. Fig. 2 illustrates two different squares, one with A-chirality and the other with B-chirality.

We model the dynamics of the dipolar square colloids using the Discontinuous Molecular Dynamics (DMD) algorithm. DMD is an accelerated variant of the standard molecular dynamics (MD) algorithm that is applied to coarse-grained versions of molecular models (51,52). Coarse-grained models are particularly useful for exploring the behavior of large systems of particles, as well as phenomena that occur at long-time scales, as they substantially reduce the overall computational time required to simulate such systems. While in standard MD, the potentials are continuous potential functions of the interparticle distance, in DMD the potentials are represented by a series of discrete changes in the potentials value (53). When a pair of particles are not at a discontinuity in the potential, the change in the potential is zero. As a result, particles in DMD do not experience any forces or acceleration. Instead, they experience impulses over an infinitesimally small period of time at the location in the discontinuity. At all other times, their velocities (magnitude and direction) are constant until they encounter a discontinuity in the interparticle potential, at which point the trajectories of the interacting particles must be adjusted. The advantage of DMD over standard MD is that, since the particles maintain a constant velocity between discontinuities, the equations of motion between discrete points in time can be solved analytically. The DMD is an event-driven algorithm operates by moving the system of particles forward in time from interaction to interaction, significantly reducing the overall computational time compared to MD (54).

The charged discs in different squares with opposite charges experience an attractive, multi-step, square well potential, while discs with the same charge experience a repulsive, multi-step, square shoulder potential. The square potentials have the same step widths, but opposite depths. The depths and widths for either potential is selected to mimic the Yukawa potential, also known as the screened Coulomb potential. The Yukawa potential represents a full-range Coulomb potential that is shielded by a layer of aqueous counterions. A screened Coulombic potential was selected instead of a full-range Coulombic potential as, in the latter case, the computationally taxing Ewald sums method is required to account for the cumulative effect of the long-range potential across periodic boundaries during molecular simulations. The Yukawa potential is defined as

$$U_{Yukawa}(r_{ij}^*) = \frac{\varepsilon}{r_{ij}^*} \exp(-\kappa^*(r_{ij}^* - 1)) \quad (1)$$

where ε is a constant with units of energy related to the interaction strength of the potential, κ^* is the reduced inverse Debye length, which represents the range of the potential and therefore the strength of the screening effect, and r_{ij}^* is the reduced distance between the two charges. Both the inverse Debye length and the interparticle distance between the two charges are reduced by the hard disc diameter σ . The parameters used to fit the square well and shoulder potentials to the Yukawa potential were selected by determining a maximum cut-off length beyond which charged spheres will not interact with each other. This maximum cut-off length was selected to be slightly less than $\sqrt{2}\sigma$, which is the distance between two similar charges when two dipolar squares are in an anti-parallel conformation. If the cut-off length is set to be greater than $\sqrt{2}\sigma$, then dipolar squares interacting via discontinuous potentials self-assemble in a manner that is significantly different from the way that they self-assemble when they interact with continuous potentials. We have estimated that a maximum cut-off length of $\sqrt{2}\sigma$ corresponds to a reduced Debye length of approximately $\kappa^* = 3.5$. The reduced temperature of our simulations is defined to be $T^* \equiv k_B T / \varepsilon$, where k_B is the Boltzmann constant and ε is the energy constant in the Yukawa potential with units of energy related to the strength of the interaction.

Hard discs from different squares interact through the reduced hard disc potential $U_{HD}^*(r_{ij}^*)$, which is defined as

$$U_{HD}^*(r_{ij}^*) \equiv \begin{cases} \infty & \text{if } r_{ij}^* \leq 1 \\ 0 & \text{if } r_{ij}^* > 1 \end{cases} \quad (2)$$

where r_{ij}^* is the reduced distance between the centers of two hard discs. Charged discs embedded in different squares interact via a four-step reduced charged disc potential $U_{CD}^*(r_{ij}^*)$, which is defined as

$$U_{CD}^*(r_{ij}^*) \equiv \begin{cases} \varepsilon_1 & \text{if } r_{ij}^* < \sigma_1 \\ \varepsilon_2 & \text{else if } r_{ij}^* < \sigma_2 \\ \varepsilon_3 & \text{else if } r_{ij}^* < \sigma_3 \\ \varepsilon_4 & \text{else if } r_{ij}^* < \sigma_4 \\ 0 & \text{else } 0 \end{cases} \quad (3)$$

where r_{ij}^* is the reduced distance between the centers of two charged discs. The potential is either attractive (square well) if the charges are of opposite sign, or repulsive (square shoulder) if the charges are of the same sign. The step depths ($\varepsilon_1 = 2.5426$, $\varepsilon_2 = 1.5916$, $\varepsilon_3 = 0.8259$, and $\varepsilon_4 = 0.3146$) and step widths ($\sigma_1 = 0.850$, $\sigma_2 = 0.950$, $\sigma_3 = 1.150$, and $\sigma_4 = 1.400$) were selected to approximate the discontinuous

interactions between charged discs to a Yukawa potential with a reduced Debye length of $\kappa^* = 3.5$ (47).

The dipoles that are embedded within each square are transversely offset from the particle's center-of-mass. We have varied the location of the dipole's charges within the square to study how the degree to which the dipole is offset from the square's center impacts its behavior. In this paper, we consider two different dipole offsets. In the first, denoted as the *standard dipole*, the charged discs are placed in the center of either of the hard discs that they are embedded in. Both charges are located equidistant from the nearest square faces that are parallel and perpendicular to the dipole. Fig. 3.a shows that the transverse distance $d_T = 0.5\sigma$ and the lateral distance $d_L = 0.5\sigma$. This dipole offset represents dipoles squares whose permanent magnetic dipole is located along one of the square faces, and is a good representation of those designed by Han *et al* (26). In the second type of dipole offset, denoted as the *offset dipole*, the charged discs are embedded such that the lateral distance is $d_L = 0.375\sigma$ and is less than the transverse distance, which remains $d_T = 0.5\sigma$. In this case, shown in Fig. 3.b, the charges are located slightly closer to the square face that is perpendicular to the direction that the dipole points than it is to the square face that is parallel to the direction that the dipole points. To model the offset dipole, two additional bonds are required for each of the charged discs to maintain their position within the square. Each charged disc is bonded to the hard disc that it is embedded inside of (with bond lengths ranging between $0.125\sigma - \delta$ and $0.125\sigma + \delta$) and to the adjacent hard disc that contains the other embedded charge (with bond lengths ranging between $1.125\sigma - \delta$ and $1.125\sigma + \delta$).

The primary difference between the standard and the offset dipole is their preference to be in anti-parallel or head-to-tail configurations with other squares of the same type. Fig. 4 illustrates the difference between standard and offset dipoles by showing diagrams and potential energy calculations between two A-chirality squares in both head-to-tail and anti-parallel configurations. Since the charged discs are embedded within hard discs, the smallest distance that the two charged discs can come to each other is determined by their distance in any direction from the edge of the hard disc that they are embedded in. In the case of the standard dipole, the charged discs are embedded in the center of the hard discs, and therefore can never come closer to each other than $r_{ij}^* = 1.00$ in either the lateral or transverse directions. As a result, squares with standard dipoles have their lowest configurational potential in an antiparallel arrangement, in which both the charges on each square have an oppositely-charged partner. In the case of the offset dipole, the closest distance that is possible between two charges is $r_{ij} = 0.75\sigma$ in the lateral direction d_L , while the closest distance in the transverse direction d_T remains $r_{ij}^* = 1.00$. As a result, two squares with offset dipoles have their lowest configurational potential in a head-to-tail arrangement.

Methods

NVT ensemble DMD simulations are performed in a 2-dimensional simulation box with periodic boundaries. Constant temperature is maintained using the Andersen thermostat, where random squares are periodically selected and every disc within that group is reassigned a unique velocity from a Boltzmann distribution (55). Canonical ensemble annealing simulations are used to investigate the equilibrium behavior of systems of dipolar squares. In annealing simulations, the system temperature is decreased in very small steps, allowing the system to equilibrate before reducing the system temperature again. For each annealing simulation, the system temperature is set to a starting value of $T^* = 1.5$ and reduced only after 200 million collision events. On average, 200 million collision events last 1000 reduced seconds. The simulation time scale is defined in seconds as $t^* = t\sqrt{\epsilon/\sigma^2} \cdot m$. We have determined that this length of time is sufficient for a system to be considered at equilibrium after a perturbation in the system temperature.

The temperature is reduced according to the following assignment strategy:

$$T^* := \begin{cases} T^* - 0.25 & \text{if } T^* > 0.5 \\ T^* - 0.0125 & \text{else if } T^* > 0.25 \\ T^* - 0.005 & \text{else if } T^* > 0.01 \end{cases} \quad (4)$$

Each annealing simulation has 70 temperature steps and cumulatively runs for over 70,000 reduced seconds. When the temperature reaches a value of $T^* = 0.01$, the simulation is finished. At this temperature the thermal forces of the system are significantly lower than the strength of the interactions between magnetic dipoles. Below this temperature, the equilibrium structures of the system do not change further. Annealing simulations were performed for each system at area fractions, ϕ , ranging from 0.05 to 0.70. We define the area fraction as the area occupied by all squares in the simulation box, including the area between the circles in the center of the square group, divided by the total area of the simulation plane. The maximum packing fraction of this system is $\phi_{max} = 0.839$.

Four order parameters were developed to quantify the clustering behavior of the squares at each temperature step during the annealing simulations. Each order parameter measures the likelihood that a square will be found in a particular type of configuration with other squares when it is at equilibrium. A value of 0 indicates that none of the squares in the system have adopted the specified conformation, while a value of 1 indicates that all squares in the system have adopted the specified conformation. The order parameters are plotted against the reduced temperature of the system over the course of an annealing simulation to determine the temperature at which the system transitions from a state in which none of the squares in the system conform to a particular order parameter to a state in which all or most of the squares in the system conform to a particular order parameter. This transition for any order parameter is defined to occur at the inflection point in the line fit to the order parameter data vs. the reduced temperature. The transition temperature of any order parameter is

determined by calculating the inflection point of the logistic5 curve fit to the order parameter data

$$\Phi(T^*) = C_1 + \frac{C_2 - C_1}{\left(1 + \left(\frac{C_3}{T^*}\right)^{C_4}\right)^{C_5}} \quad (5)$$

where T^* is the reduced temperature, $\Phi(T^*)$ is the order parameter as a function of the reduced temperature over the course of the anneal simulation, and C_1 , C_2 , C_3 , C_4 , and C_5 are constants used to fit the logistic5 curve to the order parameter data. Examples of selected order parameter data fit to the logistic5 curve are provided in the ESI.

In total we use four order parameters to categorize the phase behavior of large systems of dipolar squares. Two of the order parameters quantify how the dipolar squares aggregate with one another by measuring the configuration of squares that are associated with other squares. The other two order parameters are used to quantify the macroscopic, morphological properties of the systems of dipolar squares. For some order parameters, we use clustering criterion to determine if two squares are associated with one another. We consider two squares to be associated with one another if either of their two opposite charges are within a certain distance of one another. We define two charged discs as being associated if they are within a distance of $\sqrt{2}\sigma$ from one another, which is the maximum interaction distance of the charged disc potential. We have found that this threshold distance is a good measure of square-square association. Increasing the threshold distance beyond this value does not make sense as the charged discs would not interact with each other in that case.

The first configurational order parameter is the single-strand order parameter, $\Phi_{single-strand}$, which quantifies the extent to which a system of dipolar squares conforms to a single-stranded assembly. A square is considered in a single-stranded assembly if each of its charged discs are associated with at least one other oppositely charged disc. In a single-stranded assembly, each square aligns in a head-to-tail configuration with two other squares, as illustrated in Fig. 5. The single-strand order parameter $\Phi_{single-strand}$ is defined as the ensemble-averaged number of squares that conform to a single stranded assembly, $N_{single-strand}$, normalized by the total number of squares in the system, $N_{squares}$.

$$\Phi_{single-strand} \equiv \left\langle \frac{N_{single-strand}}{N_{squares}} \right\rangle \quad (6)$$

The second configurational order parameter is the double-strand order parameter, $\Phi_{double-strand}$, which quantifies the extent to which a system of dipolar squares conforms to a double-stranded assembly. A square is considered to be in a double-stranded assembly when each of its charged discs is

associated with two oppositely-charged discs, shown in Fig. 5. In this type of assembly, both of the charged discs embedded within a square are unable to associate with any additional charged discs, due to the steric hindrances of how the dipole is embedded in the square, and the square has reached its lowest possible potential energy. The double-strand order parameter $\Phi_{double-strand}$ is defined as the ensemble-averaged number of squares that are conform to a double-stranded assembly, $N_{double-strand}$, normalized by the total number of squares in the system, $N_{squares}$.

$$\Phi_{double-strand} = \left\langle \frac{N_{double-strand}}{N_{squares}} \right\rangle \quad (7)$$

We have defined the single- and double-stranded order parameters in such a way that for a square to meet the double-stranded order parameter criteria, it must already meet the single-stranded order parameter criteria. As a result, as any system of colloidal squares cools during an annealing simulation, the system first enters a single-stranded phase and then a double-stranded phase.

The first morphological order parameter is the percolation probability, Π , which measures the likelihood of finding a cluster of associated squares with infinite length. A system of colloidal particles that have achieved a percolated state are considered to be in a gel phase. Gel phases have a high degree of particle interconnectivity and are associated with materials that have properties such as mechanical stability or electrical conductivity (56). A system is determined to be percolated if any one cluster of squares spans the length of the periodic simulation box and connects with itself independently in both dimensions. A cluster is defined as any group of squares that are associated with each other (57). So, for example, if one square is associated with two other squares, all three squares are considered to be a part of the same cluster. The percolation parameter is a measure of whether or not a configuration of a system is in a percolated state. If the configuration at any point in time has reached a percolated state, that percolation parameter for that configuration $C_{percolated}$ is assigned a value of one. Otherwise, it is assigned a value of zero. The ensemble average of the percolation order parameter, Π , for any temperature is therefore the ensemble average of the value $C_{percolated}$ assigned to each system configuration that was examined for that ensemble.

$$\Pi \equiv \langle C_{percolated} \rangle \quad (8)$$

The second morphological order parameter is the nematic order parameter, S , which measures the directional order of the system. The nematic order parameter is calculated by measuring the angle between the embedded dipoles of every pair of squares θ_{ij} in each configurational snapshot that is taken. It is defined in a such a way that if a pair of dipoles are

aligned in a head-to-tail or antiparallel configuration ($\theta_{ij} = 0$ or $\theta_{ij} = \pi$), the order parameter has a value of 1. However, if the pair of dipoles are aligned perpendicularly ($\theta_{ij} = \pi/2$), the order parameter is $-1/2$. For any system that has a random orientational distribution, $\langle \cos^2 \theta_{ij} \rangle = 1/3$ and the nematic order parameter has a value of 0 (58).

$$S \equiv \frac{1}{2} \langle 3 \cos^2 \theta_{ij} - 1 \rangle \quad (9)$$

We define a system to be in a nematic state when the ensemble average of the nematic order parameter is $S \geq 0.8$, signifying the system's transition from a directionally disordered state into a directionally ordered state. The nematic order parameter has been used by others to study the nematic-isotropic phase transition in systems of soft ellipsoids with molecular dipoles, as well as in many other systems (59).

Results

Simulations were performed for single- and mixed-chirality systems of dipolar squares with either an embedded standard dipole or an offset one. In total, we explored four systems: 1) single-chirality systems of dipolar squares with standard dipoles, 2) mixed-chirality systems of dipolar squares with standard dipoles, 3) single-chirality systems of squares with offset dipoles, and 4) mixed-chirality systems of squares with offset dipoles. For each system, annealing simulations were performed on systems containing $N_{squares} = 1,024$ squares at excluded area fractions ranging from $\phi = 0.05$ to $\phi = 0.70$. Single chirality systems consisted entirely of A-chirality squares ($N_A = 1,024$ and $N_B = 0$), while mixed chirality systems consisted of equal numbers of A- and B-chirality squares ($N_A = 512$ and $N_B = 512$, respectively). For the remainder of this paper, we visualize the dipolar colloids as squares, rather than as the groupings of hard circles. This was done to better illustrate the results of our simulations, which were designed to model the behavior of dipolar square colloids. To do this, we used the *Open Visualization Tool* (OVITO), an open source tool for visualizing data from atomistic simulations (60).

Single-Chirality Systems of Squares with Standard Dipoles

We begin with the results of the annealing simulations performed on single-chirality systems of dipolar squares with standard dipoles. The phase diagram for this system, plotted in the area fraction vs. reduced temperature plane, is shown in Fig. 6.a. At high temperatures, the system of dipolar squares exists in an isotropic state where the squares are disordered with respect to one another and do not aggregate (Fig. 6.I). As the temperature is reduced below a threshold value, the squares begin to aggregate with each other, first forming single-stranded (Fig. 6.II), and then double-stranded (Fig. 6.III), assemblies. For this system, the transition temperatures of the single-strand and double-strand order parameters are in close

proximity to one another. This indicates that the dipolar squares rapidly coalesce into double-strands as they transition from a disordered state and begin to aggregate with mutual alignment. This phenomenon is illustrated by simulation snapshots, shown in Fig. 6.b for each phase observed and at various densities. At low temperatures (Fig. 6.III and Fig.6.IV), nearly every square is in anti-parallel alignment with another dipolar square, forming a double-stranded assembly. The double-strands that form at low densities have a rod-like morphology, are relatively inflexible, and remain disordered with respect to each other. The length of the double-strands that form depends on the system density. At low system densities, the double-strands are relatively short and as the density increases, so does their length, sometimes even reaching lengths that span the length of the simulation boxes' periodic boundaries. However, even though some double strands span the length of the simulation box, we find that the criteria for percolation are never met at any temperature or density for this system.

The double-strands tend to assemble into a nematic state, but only when the density in annealing simulation is above a threshold value (Fig. 6.IV). Even then, only a fraction of the annealing simulations performed under identical conditions form a nematic state, indicating the inconsistent nature of the formation of this phase. In the nematic phase, the dipolar squares align with one another. The nematic state only occurs for systems that are above a critical density, which corresponds to area fraction of $\phi \geq 0.60$, but not in all runs. Fig. 6.a shows the region on the phase diagram where the nematic state appears to occur; the dotted lines and question marks are meant to convey that this is a tentative result. When in the nematic state, the double-strands grow longer and tend to align as the temperature is reduced below an aggregation threshold temperature, and the system's potential energy is significantly lower than in the non-nematic state. The likelihood of forming a nematic state increases as the system density increases. We have not yet been able to determine a set of conditions when the nematic state appears consistently. When we increased the length of each temperature step from 200 million events to 1 billion events (see (4)), the system was more likely to form a nematic state, but it still did not do this consistently. Thus, at this point in time, we conclude that more sophisticated methods, which are beyond the scope of this paper, will be required to pinpoint the formation of a nematic state by these dipolar squares. Additional information about the probability and frequency of the formation of a nematic state for this system have been included in the Electronic Supplementary Information.

Mixed-Chirality Systems of Squares with Standard Dipoles

The second system that we explored is a mixed-chirality system of squares with standard dipoles. The phase diagram for this system, plotted in the area fraction vs. reduced temperature plane, is shown in Fig. 7.a. The phase behavior of these systems is very similar to that of the single chirality systems of squares with standard dipoles just discussed. At high temperatures, the squares exist in an isotropic fluid state where

they are disordered with respect to one another and do not aggregate (Fig. 7.I). As the temperature is reduced below a threshold value, the squares begin to aggregate, first forming single-stranded, then double-stranded assemblies (Fig. 7.II and Fig. 7.III, respectively). Once again, the transition temperatures of the single-stranded and double-stranded phases are in close proximity to one another, indicating that as the temperature is reduced below a threshold value the squares quickly assemble into double-strands. This is illustrated by simulation snapshots shown in Fig. 7.b for each phase observed and at various densities.

We find that for this system two different types of double-stranded assemblies form. The first double-stranded assembly consists exclusively of one type of square, either A-chirality or B-chirality. This homogeneous double-stranded assembly is like those observed in the single chirality system of squares with standard dipoles: two strands of squares with the same chirality coalesce such that their dipoles point antiparallel to one another. The second type of double-stranded assembly consists of both A- and B-chirality squares. In a heterogeneous double-stranded assembly, two strands made from squares with opposite chiralities coalesce such that their dipoles point in the same direction with respect to one another. Simulation snapshots in Fig. 7.b at low temperatures (Fig. 7.III) illustrate the difference between these two different types of double-stranded assemblies, while Fig. 5 shows how a double-stranded assembly can form from either a single-chirality square or from a mixture of both chiralities of square. Unlike the previous system, the nematic order parameter remains at a constant value of approximately $S \approx 0.25$ for all system temperatures and densities, indicating that the system remains isotropic, even at high densities. Additionally, the criteria for percolation are never met for any temperature or density for this system.

Single-Chirality Systems of Squares with Offset Dipoles

The third system explored is a single-chirality system of squares with offset dipoles. The phase diagram for this system, plotted in the area fraction vs. reduced temperature plane, is shown in Fig. 8.a. At high temperatures, the system of squares exists in an isotropic, fluid state where the squares are disordered with respect to one another and do not aggregate. As the temperature is reduced, the squares begin to aggregate (Fig. 8.I). We notice two distinct differences in their aggregation behavior compared to that of systems of squares with standard dipoles. First, the temperature at which the squares begin to aggregate is significantly higher. Second, the single- and double-stranded phase transition temperatures occur at considerably different values from each other at all area fractions, unlike what occurs in the standard dipoles case. While the transition temperatures of the double-stranded order parameter are approximately the same as for systems of squares with standard dipoles, the single-stranded order parameter transition temperatures are all significantly higher. As a result, the portion of the phase diagram for this system corresponding to the single-stranded phase is significantly wider than the same region of the phase diagram for systems of squares with

standard dipoles, while the portion of the phase diagram corresponding to the double-stranded phases is approximately the same area as the previous systems.

The morphology and macroscopic assemblies of systems of squares with offset dipoles are different from those for systems of squares with standard dipoles. This can be seen by examining simulation snapshots shown in Fig. 8.b. At temperatures corresponding to the "Single-Stranded Fluid" region of the phase diagram (Fig. 8.II), the squares form long chains and ring-like or cyclical structures in which all the squares are in head-to-tail configurations with one another. As the temperature is reduced further into the "Double-Stranded Fluid" region of the phase diagram (Fig. 8.III), double-stranded assemblies form, however they are shorter than those for the dipolar squares with standard dipoles and are often attached to short chains of single-stranded assemblies. The nematic order parameter remains constant at a value of approximately $S \approx 0.25$ for all system temperatures and densities, indicating that the system remains isotropic, even at high densities. Additionally, the criteria for percolation are not met at any temperature or density.

Mixed-Chirality Systems of Squares with Offset Dipoles

The fourth and final system explored is a mixed-chirality system of squares with offset dipoles. The phase diagram for these systems plotted in the area fraction vs. reduced temperature plane is shown in Fig. 9.a. The phase behavior of these systems is similar to those for the single chirality systems of squares with offset dipoles just discussed. At high temperatures, the system of squares exists in an isotropic, fluid state where the squares are disordered with respect to one another and do not aggregate (Fig. 9.I). As the temperature is reduced, the dipolar squares begin to aggregate with one another. Similar to the single-chirality system of squares with offset dipoles, the single- and double-stranded order parameter transition temperatures are significantly different from each other at all area fractions. As a result, the single-stranded phase is considerably wider than the same region of the phase diagram for systems of squares with standard dipoles (Fig. 9.II and Fig. 9.IV), while the portion of the phase diagram corresponding to the double-stranded phases is approximately the same area as the previous systems (Fig. 9.III and Fig. 9.V).

For this system, we observe the formation of a percolated state, unlike all the previous systems that we have examined. For systems that are above a threshold density, as the temperature is reduced below the threshold aggregation temperature, the criterion for percolation is met when the area fraction of the annealing simulation is at or above $\phi = 0.25$. We consider this state to be a gel because the colloidal particles are dynamically arrested due to their strong associations with one another. Simulation snapshots, shown Fig. 9.b, illustrate this. At densities above the percolation threshold, the squares achieve a high degree of interconnectivity with assemblies that span the length of the simulation box in both dimensions. In this case, as the temperature is reduced during the annealing simulation, the system transitions from a non-percolated, single-stranded

fluid (Fig. 9.II) to a percolated, single-stranded gel (Fig. 9.IV), and remains percolated as the system transitions to a double stranded gel (Fig. 9.V). We note that at densities above or below the percolation threshold, the squares assemble into flexible, strand-like morphologies that contain approximately equal amounts of either chirality square. However, at densities below the percolation threshold, the squares are unable to percolate due to the short length of their assemblies relative to the length of the simulation box. The nematic order parameter remains constant at a value of approximately $S \approx 0.25$ for all system temperatures and densities, indicating that the squares do not align with each other, even at high densities.

Conclusions

In this study, we have performed coarse-grained molecular dynamics simulations of square colloids with magnetically-polarized dipoles that are transversely offset from their center of mass. We represent the square colloids as four hard circles that are bonded together in a rigid square geometry. The intrinsic dipole was mimicked by embedding equal but opposite charges in the hard circles, with additional bonds to maintain the position of the charges within the square geometry. Annealing simulations were performed for large numbers of the dipolar square colloids to discover their self-assembling behavior as the system temperature is slowly reduced relative to the strength of the embedded dipole. Order parameters were developed to quantify the aggregation of the squares, and subsequently to calculate phase diagrams that describe the equilibrium configurations of a system of dipolar squares at any temperature or density. We used our model to explore four different systems, which vary in type of dipole embedded within the square (either a standard or an offset dipole) and in the relative amount of opposite chirality squares present in the system.

We find that the phase diagrams for each system are unique. The microscopic configurations of the dipolar square colloids depend on the type of dipole that is embedded within the square. The microscopic configurations of the squares, in turn, determine the system's morphology and the macroscopic assemblies that the system forms at low temperatures when the strength of the embedded magnetic dipole dominates. In this paper we consider colloidal squares whose dipole has been transversely-shifted from the particle's center of mass. By adjusting the location of the transversely shifted dipole within the square, we also adjust the macroscopic structure of the system's colloidal assemblies, and therefore alter the dipolar square's preference for anti-parallel or head-to-tail microscopic configurations with other squares. Squares with standard dipoles prefer antiparallel configurations with other dipolar squares. They assemble into rod-like structures that are linear and have a rigid morphology. Alternatively, squares with offset dipoles prefer head-to-tail configurations with other dipolar squares. Systems of squares with offset dipoles assemble into single-stranded assemblies with string-like morphologies. Single-stranded assemblies are relatively flexible in comparison to double-stranded assemblies.

The simulations predict that the dipolar squares with transversely offset dipoles exhibit two unique density-dependent phase transitions, to either nematic or percolated states, although the transition to the nematic state is not seen consistently in all runs. The type of transition that occurs, nematic or percolated, depends not only on how the dipole is embedded within the square, but also on the presence or absence of opposite chirality squares within the system. Systems of squares with offset dipoles exhibit a percolation transition at low temperatures and moderate-to-high densities. In a percolated state, the dipolar colloids have a high degree of interconnectivity and form clusters that span the entire length of the simulation box. This is likely a result of the propensity of the chiral mixtures to form linear chains, rather than anti-parallel doublets (cf. Fig. 8 and Fig. 9). However, the percolation transition only occurs for systems of squares that contain equal numbers of either chirality of square. Systems of the same squares that contain only one chirality are unable to percolate under the same conditions. Additionally, systems of squares with standard dipoles sometimes formed a nematic state at high densities. We are unable to conclusively verify that the nematic state is the system's most stable configuration due to the inconsistent results from the annealing simulation, as described in the results section. At high densities and low temperatures, double-stranded assemblies in the system become oriented in the same direction due to the excluded-volume interactions of the rods. However, the nematic state only occurs for systems of squares with standard dipoles that contain only one chirality square. Even though mixed chirality systems of squares with standard dipoles form the same rod-like structures as single-chirality systems, we never observe them to form a globally aligned state under the same conditions.

The difficulty of reliably obtaining a nematic state at the end of an annealing simulation is not surprising given the system's high densities and low temperatures, hallmarks of glassy dynamics. In the glassy state, the strong interactions between particles significantly increase the time required to fully explore all of the system's configurational possibilities. Based on the inconsistent behavior in the annealing simulations not only as a function of system parameters (i.e. temperature, density), but also of the length of the annealing simulation at each temperature step, we expect that there exists a free energy barrier that prevents the system from transitioning to a nematic state and that the size of this barrier decreases as the system's density increases. Below area fractions of 0.60, the barrier is too large for the system to transition to a nematic state. If annealing simulations for this system for area fractions at or above 0.60 were run sufficiently (or infinitely) long at each temperature step, we expect that the system would reliably assemble into a nematic state. In that case the system would have enough time to sufficiently explore all configurational possibilities and likely find the most stable arrangement under those conditions. Additional information about the frequency and probability of the occurrence of a nematic state have been included in the Electronic Supplementary Information. In future work, we hope

to further explore this issue with algorithms that are better suited for calculating the system's free energy.

The dimensions and length scales of the box that we have used for our simulations could have an impact on which density-dependent phases we observe in our simulations. Simulations are subject to density fluctuations up to the length scale of the periodic box boundaries but are unable to capture the occurrence of longer-wavelength density fluctuations, which influence both the percolated and nematic states (61). For example, as the single-chirality system of squares with standard dipoles transitions from a double-stranded fluid to a nematic state, there is likely an interface that occurs between the disordered liquid state and the ordered crystal state. For this interface to be properly observed, the dimensions of the box should be significantly greater than the length scale of the liquid-solid interface. If one box dimension was significantly longer than the other, this would enhance the likelihood that the solid-liquid phase interface would form, making it easier to observe the order-disorder transition (62). The simulation box dimensions could also impact the likelihood of percolation, especially close to the transition point when the formation of a percolated state is less stable. We will consider this for future work.

In our computational studies, simulations are performed in two-dimensions and, as a result, the relative number of chiral particles present in the system remain fixed. In experimental system, the chirality of any particle would be able to change should sufficient energy allow particle to flip or rotate onto another side. Our results suggest that at low to moderate densities, squares with offset dipoles confined to a plane would prefer to form a racemic mixture, and under certain conditions would form a high-interconnected, gel-like state. At high densities, however, the racemic mixture of dipolar squares is unable to form an order state. Instead, our results suggest, although do not prove, that the system may prefer configurations containing only one chirality of square. This information suggests that one might be able to control the relative amounts of chiral squares by adjusting the system density. An interesting avenue of further study would be to employ mixed DMD-MC simulations in which the chirality of the particle is allowed to flip according to some acceptance criteria (63).

The information provided by our computational investigation is useful for colloidal scientists synthesizing new types of particles. To the best of our knowledge, we are the first to perform theoretical studies of square particles with transversely shifted dipoles. We have discovered that the phase behavior of squares with transversely shifted magnetic dipoles is diverse, as they exhibit unique phases and morphologies that are sensitive to the location of the dipole embedded within them. Our inspiration for creating this model was the cubic microparticles synthesized by Han *et al.*, which have one face that is coated in a polarizable magnetic material (26). We believe that our squares with standard dipoles provide guidelines for further investigations of the behavior of such emerging systems of microparticles with complex shape and interactions. We have shown how these colloids assembly into

rods with linear and rigid morphologies, and exhibit temperature and density-dependent phase transitions, including the formation of a nematic phase under certain conditions.

We also are interested in colloidal systems with highly interconnected gel-like states, as these phases are correlated with potentially desirable material properties. For this reason, we adjusted the standard dipole to create the offset dipole. This adjustment is experimentally analogous to taking the particles synthesized by Han *et al.* and shifting the magnetic dipole slightly away from the face and towards the square's center. We found that by adjusting the location of the magnetic dipole within the square colloid, we switched the configurational preference of the squares in our model from anti-parallel to head-to-tail. This adjustment resulted in a remarkable shift in the system's morphology, to more flexible assemblies, and phase behavior, enabling the formation of a percolated, gel-like state. While particles like this have not yet been realized experimentally, we believe that their interesting structural properties make them an exciting possibility and that their synthesis should be pursued by colloidal scientists for verification.

The use of Discontinuous Molecular Dynamics (DMD) to model the polarized, square microparticles was driven by our goal of exploring the large phase space of systems of square-shaped particles. The advantage of DMD is that we can rapidly simulate systems under many different conditions using only modest computational resources. Additionally, we were able to use simple DMD techniques to construct models of particles that have anisotropic interactions by applying isotropic interactions in specific ways. The use of short-ranged potentials also increases the computational speed of our simulations, allowing us to avoid using the computationally-costly Ewald sums method. While our model does not account for the effect of long-ranged potentials, we expect that the results of our study are qualitatively correct. The implementation of long-ranged interactions would likely result in transitions that occur at different temperatures, as the squares would aggregate or percolate sooner in the annealing simulations. We believe that our efforts to model square colloidal particles with transversely-offset dipoles will help guide experimentalists towards new and exciting colloidal particle systems with unique assembly properties and phases.

Author Contributions

Matthew A. Dorsey: Conceptualization, Methodology, Software, Formal Analysis, Investigation, Visualization, Writing – Original Draft

Orlin D. Velev: Writing – Review & Editing, Supervision, Funding Acquisition

Carol K. Hall: Writing – Review & Editing, Supervision, Project Administration, Funding Acquisition

Conflicts of interest

There are no conflicts to declare.

Acknowledgements

This research was supported by NSF grant number CBET-1935248. We acknowledge the computing resources provided by North Carolina State University High Performance Computing Services Core Facility (RRID:SCR_022168), as well as the staff who helped facilitate this project. We also acknowledge that a portion of this research was completed using services provided by the OSG Consortium (64,65), which is supported by the National Science Foundation awards #2030508 and #1836650.

Notes and references

- Boles MA, Engel M, Talapin DV. Self-Assembly of Colloidal Nanocrystals: From Intricate Structures to Functional Materials. *Chem Rev.* 2016 Sep 28;116(18):11220–89.
- Yethiraj A, van Blaaderen A. A colloidal model system with an interaction tunable from hard sphere to soft and dipolar. *Nature.* 2003 Jan;421(6922):513–7.
- Mitragotri S, Lahann J. Physical approaches to biomaterial design. *Nat Mater.* 2009 Jan;8(1):15–23.
- Caruso F, Caruso RA, Möhwald H. Nanoengineering of Inorganic and Hybrid Hollow Spheres by Colloidal Templating. *Science.* 1998;282(5391):1111–4.
- Giljohann DA, Seferos DS, Daniel WL, Massich MD, Patel PC, Mirkin CA. Gold Nanoparticles for Biology and Medicine. *Angew Chem Int Ed.* 2010;49(19):3280–94.
- Baumgartl J, Zvyagolskaya M, Bechinger C. Tailoring of Phononic Band Structures in Colloidal Crystals. *Phys Rev Lett.* 2007 Nov 14;99(20):205503.
- Hynninen AP, Thijssen JHJ, Vermolen ECM, Dijkstra M, van Blaaderen A. Self-assembly route for photonic crystals with a bandgap in the visible region. *Nat Mater.* 2007 Mar;6(3):202–5.
- Kredentser S, Buluy O, Davidson P, Dozov I, Malynych S, Reshetnyak V, et al. Strong orientational coupling in two-component suspensions of rod-like nanoparticles. *Soft Matter.* 2013;9(20):5061–6.
- Li Y, Cai W, Duan G. Ordered Micro/Nanostructured Arrays Based on the Monolayer Colloidal Crystals. *Chem Mater.* 2008 Feb 1;20(3):615–24.
- Chen Y, Ding X, Steven Lin SC, Yang S, Huang PH, Nama N, et al. Tunable Nanowire Patterning Using Standing Surface Acoustic Waves. *ACS Nano.* 2013 Apr 23;7(4):3306–14.
- Milliron DJ, Hughes SM, Cui Y, Manna L, Li J, Wang LW, et al. Colloidal nanocrystal heterostructures with linear and branched topology. *Nature.* 2004 Jul;430(6996):190–5.
- Phillips CL, Jankowski E, Krishnatreya BJ, Edmond KV, Sacanna S, Grier DG, et al. Digital colloids: reconfigurable clusters as high information density elements. *Soft Matter.* 2014 Sep 10;10(38):7468–79.
- Liang X, Dong R, Ho JC. Self-Assembly of Colloidal Spheres toward Fabrication of Hierarchical and Periodic Nanostructures for Technological Applications. *Adv Mater Technol.* 2019;4(3):1800541.
- Glotzer SC, Solomon MJ. Anisotropy of building blocks and their assembly into complex structures. *Nat Mater.* 2007 Aug;6(8):557–62.
- Walther A, Müller AHE. Janus Particles: Synthesis, Self-Assembly, Physical Properties, and Applications. *Chem Rev.* 2013 Jul 10;113(7):5194–261.
- Frenkel D. Entropy-driven phase transitions. *Phys Stat Mech Its Appl.* 1999 Feb 1;263(1):26–38.
- Li ZW, Lu ZY, Sun ZY, An LJ. Model, self-assembly structures, and phase diagram of soft Janus particles. *Soft Matter.* 2012;8(25):6693.
- Gröschel AH, Löbbling TI, Petrov PD, Müllner M, Kuttner C, Wieberger F, et al. Janus Micelles as Effective Supracolloidal Dispersants for Carbon Nanotubes. *Angew Chem Int Ed.* 2013;52(13):3602–6.
- Velev OD, Gangwal S, Petsev DN. Particle-localized AC and DC manipulation and electrokinetics. *Annu Rep Sect C Phys Chem.* 2009;105:213.
- Gangwal S, Pawar A, Kretzschmar I, Velev OD. Programmed assembly of metalodielectric patchy particles in external AC electric fields. *Soft Matter.* 2010;6(7):1413.
- Novak EV, Pyanzina ES, Kantorovich SS. Behaviour of magnetic Janus-like colloids. *J Phys Condens Matter.* 2015 May;27(23):234102.
- Smoukov SK, Gangwal S, Marquez M, Velev OD. Reconfigurable responsive structures assembled from magnetic Janus particles. *Soft Matter.* 2009;5(6):1285.
- Gangwal S, Cayre OJ, Velev OD. Dielectrophoretic Assembly of Metalodielectric Janus Particles in AC Electric Fields. *Langmuir.* 2008 Dec 2;24(23):13312–20.
- Iv CWS, Zhu S, Yang Y, Bharti B, Liu J, Yellen BB, et al. Field-directed assembly of patchy anisotropic microparticles with defined shape. *Soft Matter.* 2013 Sep 12;9(38):9219–29.
- Patti A, Cuetos A. Brownian dynamics and dynamic Monte Carlo simulations of isotropic and liquid crystal phases of anisotropic colloidal particles: A comparative study. *Phys Rev E.* 2012 Jul 9;86(1):011403.
- Han K, Shields CW, Diwakar NM, Bharti B, López GP, Velev OD. Sequence-encoded colloidal origami and microbot assemblies from patchy magnetic cubes. *Sci Adv.* 2017 Aug 4;3(8):e1701108.
- Han K, Shields CW, Bharti B, Arratia PE, Velev OD. Active Reversible Swimming of Magnetically Assembled “Microscallops” in Non-Newtonian Fluids. *Langmuir.* 2020 Jun 30;36(25):7148–54.
- Shields IV CW, Kim YK, Han K, Murphy AC, Scott AJ, Abbott NL, et al. Control of the Folding Dynamics of Self-Reconfiguring Magnetic Microbots Using Liquid Crystallinity. *Adv Intell Syst.* 2020;2(2):1900114.
- Alarcón-Waess O. The role played by self-orientational properties in nematics of colloids with molecules axially symmetric. *J Chem Phys.* 2010 Apr 14;132(14):144902.
- John BS, Juhlin C, Escobedo FA. Phase behavior of colloidal hard perfect tetragonal parallelepipeds. *J Chem Phys.* 2008 Jan 28;128(4):044909.
- Dussi S, Tasios N, Drwenski T, van Roij R, Dijkstra M. Hard Competition: Stabilizing the Elusive Biaxial Nematic Phase in Suspensions of Colloidal Particles with Extreme Lengths. *Phys Rev Lett.* 2018 Apr 24;120(17):177801.
- Patti A, Cuetos A. Monte Carlo simulation of binary mixtures of hard colloidal cuboids. *Mol Simul.* 2018 Apr 13;44(6):516–22.
- Zöttl A, Stark H. Emergent behavior in active colloids. *J Phys Condens Matter.* 2016 May;28(25):253001.
- Patti A, Cuetos A. Dynamics of colloidal cubes and cuboids in cylindrical nanopores. *Phys Fluids.* 2021 Sep;33(9):097103.
- Mirzad Rafaeel E, Corbett D, Cuetos A, Patti A. Self-assembly of freely-rotating polydisperse cuboids: unveiling the boundaries of the biaxial nematic phase. *Soft Matter.* 2020;16(24):5565–70.
- M. Rutkowski D, D. Velev O, L. Klapp SH, K. Hall C. Simulation study on the structural properties of colloidal particles with offset dipoles. *Soft Matter.* 2017;13(17):3134–46.

- 37 Linse P. Quasi-2d fluids of dipolar superballs in an external field. *Soft Matter*. 2015;11(19):3900–12.
- 38 Rao Vutukuri H, Smallemburg F, Badaire S, Imhof A, Dijkstra M, Blaaderen A van. An experimental and simulation study on the self-assembly of colloidal cubes in external electric fields. *Soft Matter*. 2014;10(45):9110–9.
- 39 Tonti L, García Daza FA, Patti A. Kinetics of isotropic to string-like phase switching in electrorheological fluids of nanocubes. *J Chem Phys*. 2022 Dec 14;157(22):224906.
- 40 Kwaadgras BW, van Roij R, Dijkstra M. Self-consistent electric field-induced dipole interaction of colloidal spheres, cubes, rods, and dumbbells. *J Chem Phys*. 2014 Apr 21;140(15):154901.
- 41 Cuetos A, Mirzad Rafael E, Corbett D, Patti A. Biaxial nematics of hard cuboids in an external field. *Soft Matter*. 2019;15(9):1922–6.
- 42 John BS, Stroock A, Escobedo FA. Cubatic liquid-crystalline behavior in a system of hard cuboids. *J Chem Phys*. 2004 May 15;120(19):9383–9.
- 43 Avendaño C, A. Escobedo F. Phase behavior of rounded hard-squares. *Soft Matter*. 2012;8(17):4675–81.
- 44 G. Donaldson J, S. Kantorovich S. Directional self-assembly of permanently magnetised nanocubes in quasi two dimensional layers. *Nanoscale*. 2015;7(7):3217–28.
- 45 Pyanzina ES, Gudkova AV, Donaldson JG, Kantorovich SS. Cluster analysis in systems of magnetic spheres and cubes. *J Magn Magn Mater*. 2017 Jun 1;431:201–4.
- 46 Goyal A, Hall CK, Velev OD. Phase diagram for stimulus-responsive materials containing dipolar colloidal particles. *Phys Rev E*. 2008 Mar 3;77(3):031401.
- 47 Rutkowski DM, Velev OD, Klapp SHL, Hall CK. The effect of charge separation on the phase behavior of dipolar colloidal rods. *Soft Matter*. 2016;12(22):4932–43.
- 48 Maloney RC, Hall CK. Phase diagrams of mixtures of dipolar rods and discs. *Soft Matter*. 2018;14(38):7894–905.
- 49 Bellemans A, Orban J, Van Belle D. Molecular dynamics of rigid and non-rigid necklaces of hard discs. *Mol Phys*. 1980 Feb 20;39(3):781–2.
- 50 Mahynski NA, Shen VK. Symmetry-derived structure directing agents for two-dimensional crystals of arbitrary colloids. *Soft Matter*. 2021;17(34):7853–66.
- 51 Rapaport DC. Molecular dynamics study of a polymer chain in solution. *J Chem Phys*. 1979 Oct 15;71(8):3299–303.
- 52 Cheon M, Chang I, Hall CK. Extending the PRIME model for protein aggregation to all 20 amino acids. *Proteins Struct Funct Bioinforma*. 2010;78(14):2950–60.
- 53 Alder BJ, Wainwright TE. Studies in Molecular Dynamics. I. General Method. *J Chem Phys*. 1959 Aug;31(2):459–66.
- 54 Smith SW, Hall CK, Freeman BD. Molecular Dynamics for Polymeric Fluids Using Discontinuous Potentials. *J Comput Phys*. 1997 Jun;134(1):16–30.
- 55 Andersen HC. Molecular dynamics simulations at constant pressure and/or temperature. *J Chem Phys*. 1980 Feb 15;72(4):2384–93.
- 56 Neitsch H, Klapp SHL. Percolation transition of short-ranged square well fluids in bulk and confinement. *J Chem Phys*. 2013 Feb 14;138(6):064904.
- 57 Livraghi M, Höllring K, Wick CR, Smith DM, Smith AS. An Exact Algorithm to Detect the Percolation Transition in Molecular Dynamics Simulations of Cross-Linking Polymer Networks. *J Chem Theory Comput*. 2021 Oct 12;17(10):6449–57.
- 58 Prost PG de G and J. The physics of liquid crystals. 2nd ed. Oxford: Clarendon Press ; New York : Oxford University Press, 1993.; 1993. (International series of monographs on physics ; 83).
- 59 Decoster D, Constant E, Constant M. Computer Simulation of Molecular Dynamics of Anisotropic Fluids. *Mol Cryst Liq Cryst*. 1983 Jul;97(1):263–76.
- 60 Stukowski A. Visualization and analysis of atomistic simulation data with OVITO—the Open Visualization Tool. *Model Simul Mater Sci Eng*. 2010 Jan 1;18(1):015012.
- 61 Allen MP, Tildesley DJ. Computer simulation of liquids. Second edition. Oxford, United Kingdom: Oxford University Press; 2017. 626 p.
- 62 Noya EG, Vega C, de Miguel E. Determination of the melting point of hard spheres from direct coexistence simulation methods. *J Chem Phys*. 2008 Apr 21;128(15):154507.
- 63 Kenkare NR, Hall CK, Khan SA. Theory and simulation of the swelling of polymer gels. *J Chem Phys*. 2000 Jul;113(1):404–18.
- 64 Pordes R, Petravick D, Kramer B, Olson D, Livny M, Roy A, et al. The open science grid. *J Phys Conf Ser*. 2007 Jul 1;78:012057.
- 65 Sfiligoi I, Bradley DC, Holzman B, Mhashilkar P, Padhi S, Wurthwein F. The Pilot Way to Grid Resources Using glideinWMS. In: 2009 WRI World Congress on Computer Science and Information Engineering. 2009. p. 428–32.

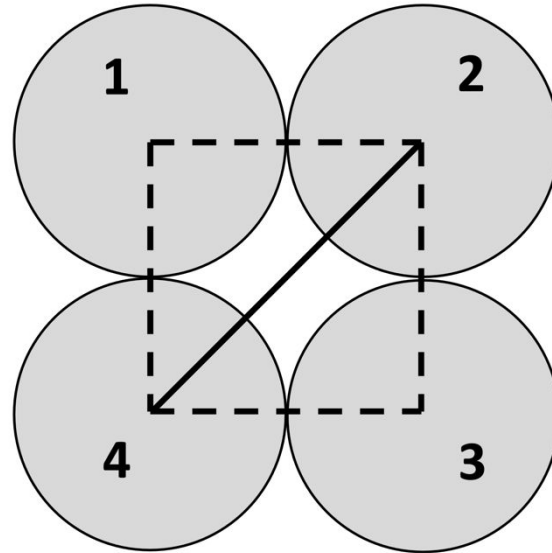


Fig. 1 Illustration of the bonding strategy used to maintain the square geometry in DMD. Four bonds (dashed black lines) link each disc with its immediate neighbor. One bond (solid black line) links one disc to the disc that is across from it.

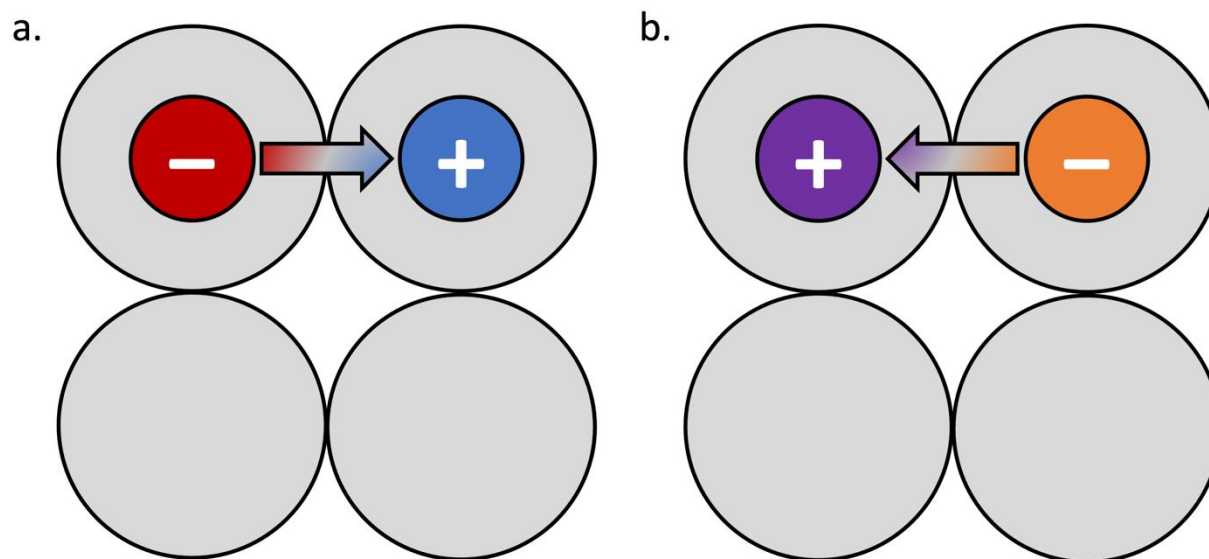


Fig. 2 Two dipolar squares with opposite chiralities are shown. (a) A dipolar square with a dipole that points clockwise relative to the square's center. This type of square is denoted A-chirality. (b) A dipolar square with a dipole that points counterclockwise relative to the square's center. This type of square is denoted B-chirality. While the opposite charges that are embedded within either of the two squares are the same, different colors are used to make distinctions between the two different squares.

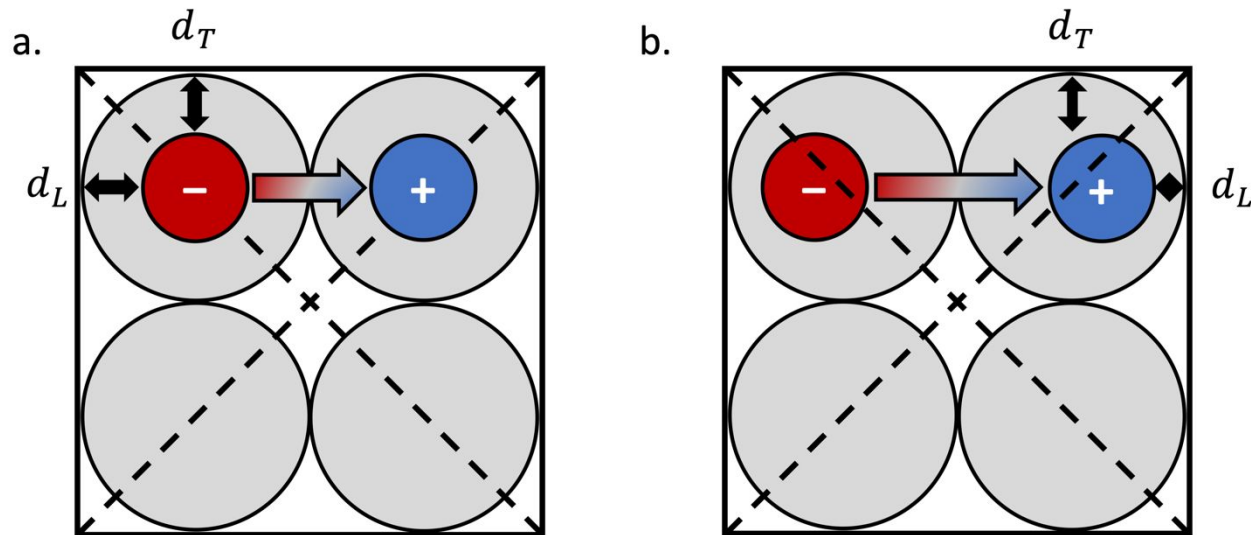


Fig. 3 Two A-chirality, dipolar squares are shown. Solid lines surround each square and illustrate the hard, square figure that the formation of hard discs represents, and dashed black lines connect opposite vertices of the square. The type of dipole that is embedded within the square is quantified by two parameters. The transverse distance (d_T) is the distance from the dipole center to the square edge that is parallel to the direction that the dipole points. The lateral distance (d_L) is the distance from the end of the dipole (either of the charged spheres) to the square edge that is perpendicular to the direction that the dipole points. (a) A dipolar square with an embedded standard dipole; the transverse distance and the lateral distance are equal. (b) A dipolar square with an embedded offset dipole; the lateral distance is slightly smaller than the transverse distance, which means that the charges on the offset dipole are slightly closer to the perpendicular square edge than to the parallel one.

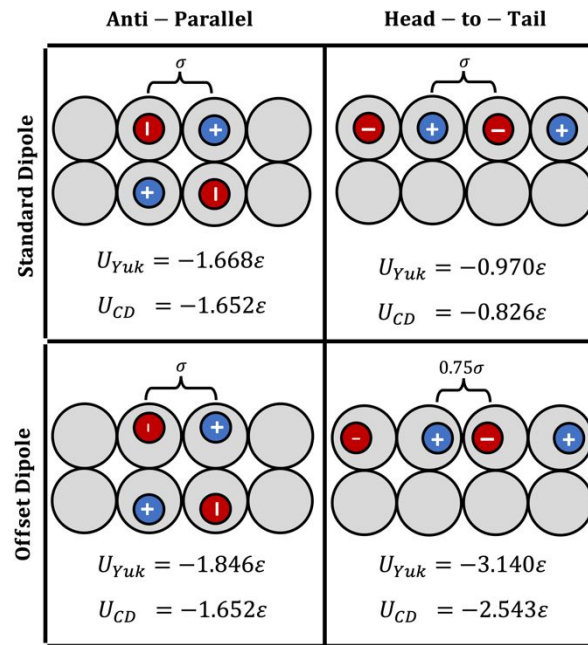


Fig. 4 Interaction potential between two polarized squares with standard (top) or offset (bottom) dipoles in anti-parallel (left) or head-to-tail (right) conformations. Each diagram lists the total interaction potentials between the two squares with charged spheres interacting via a continuous Yukawa potential U_{Yukawa} and the discontinuous potential U_{CD} that was selected to mimic the Yukawa potential.

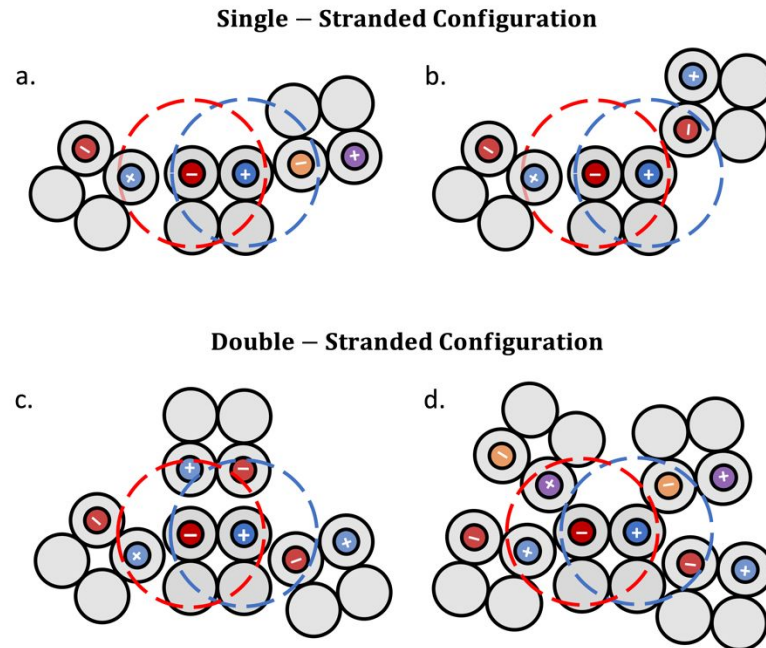


Fig. 5 Diagrams which demonstrate the possible conformations of any one square that meet the criteria for the single- (a and b) or double-stranded (c and d) order parameters. The gray circles represent the hard disks that make up the square geometry. The red and blue circles represent the centers of the negative and positive charges, respectively, embedded within A-chirality squares, and the orange and purple circles represent the negative and positive charges, respectively, embedded within B-chirality squares. The squares whose order parameter is being considered are shown in dark gray, while the squares associated with them are shown in light gray. The dashed, colored rings are centered around charged spheres corresponding to their color and are at the maximum distance at which the two opposite charges are considered to be associated with one another (the outermost well of the U_{CD} potential).

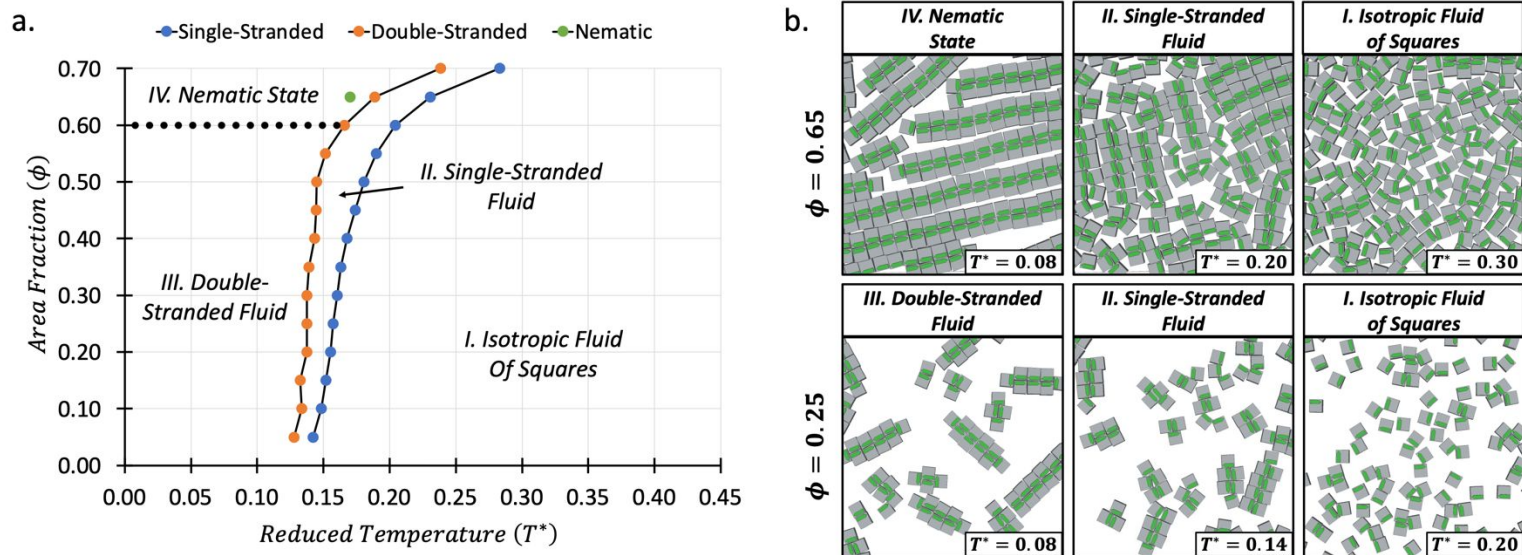


Fig. 6 (a) Phase diagram in the area fraction vs. reduced temperature plane for single-chirality systems of squares with standard dipoles. In the phase diagram, the dotted line represents the system's density threshold required for the system to form a nematic state. Below the dashed line the system will not form a nematic state while above the dashed line the system sometimes forms a nematic state. (b) Simulation snapshots show structural properties of single-chirality systems of squares with standard dipoles at various densities and temperatures. In each snapshot, squares are gray; the A-chirality squares have dipoles shown as green arrows.

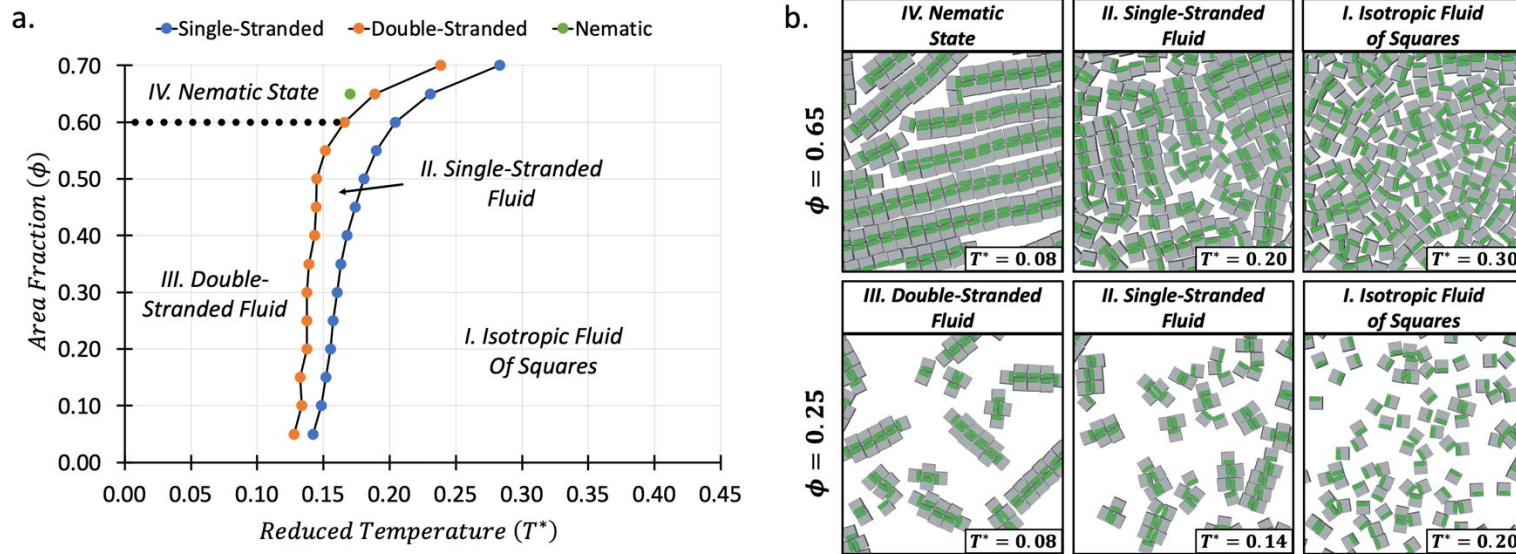
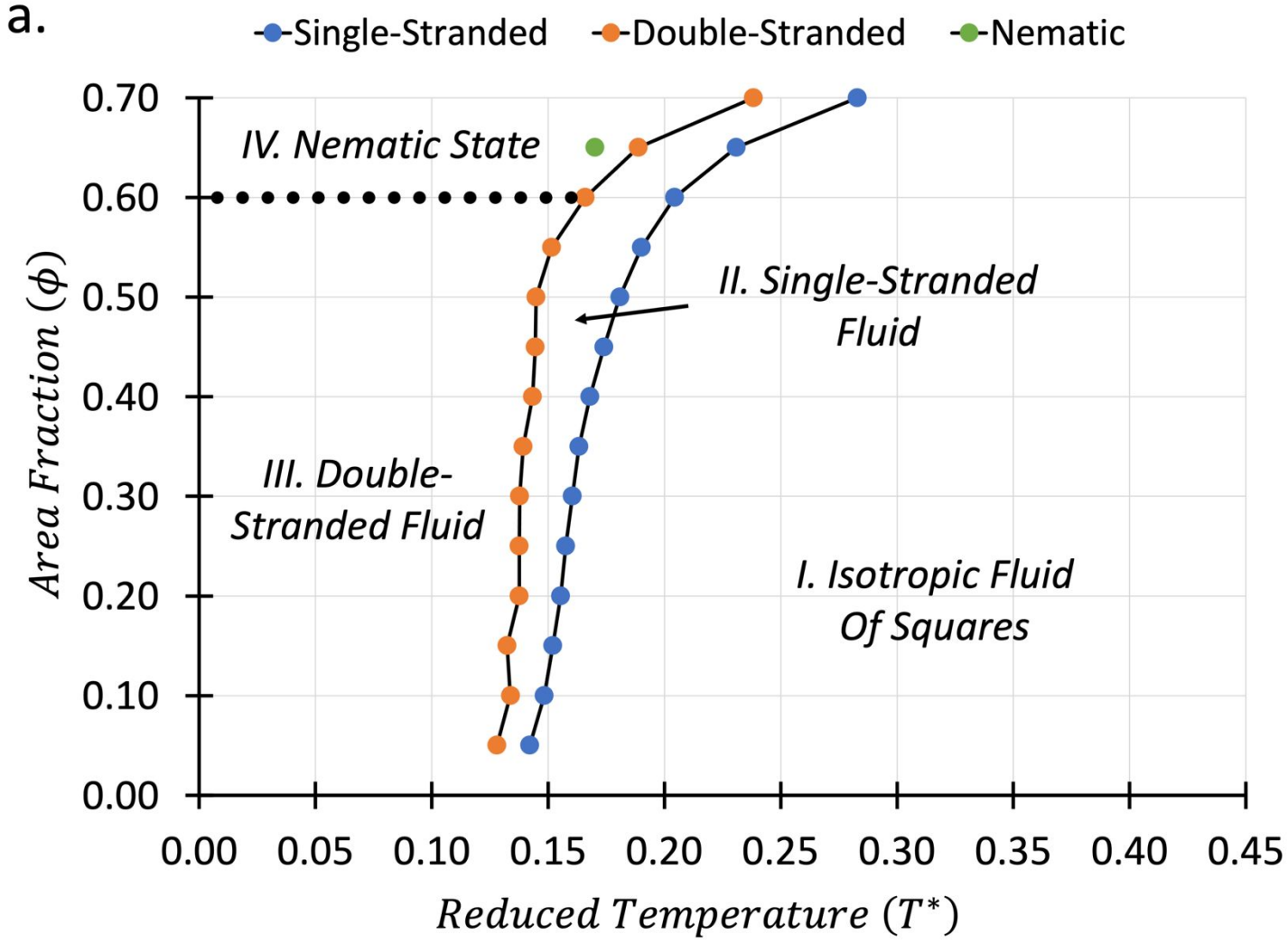
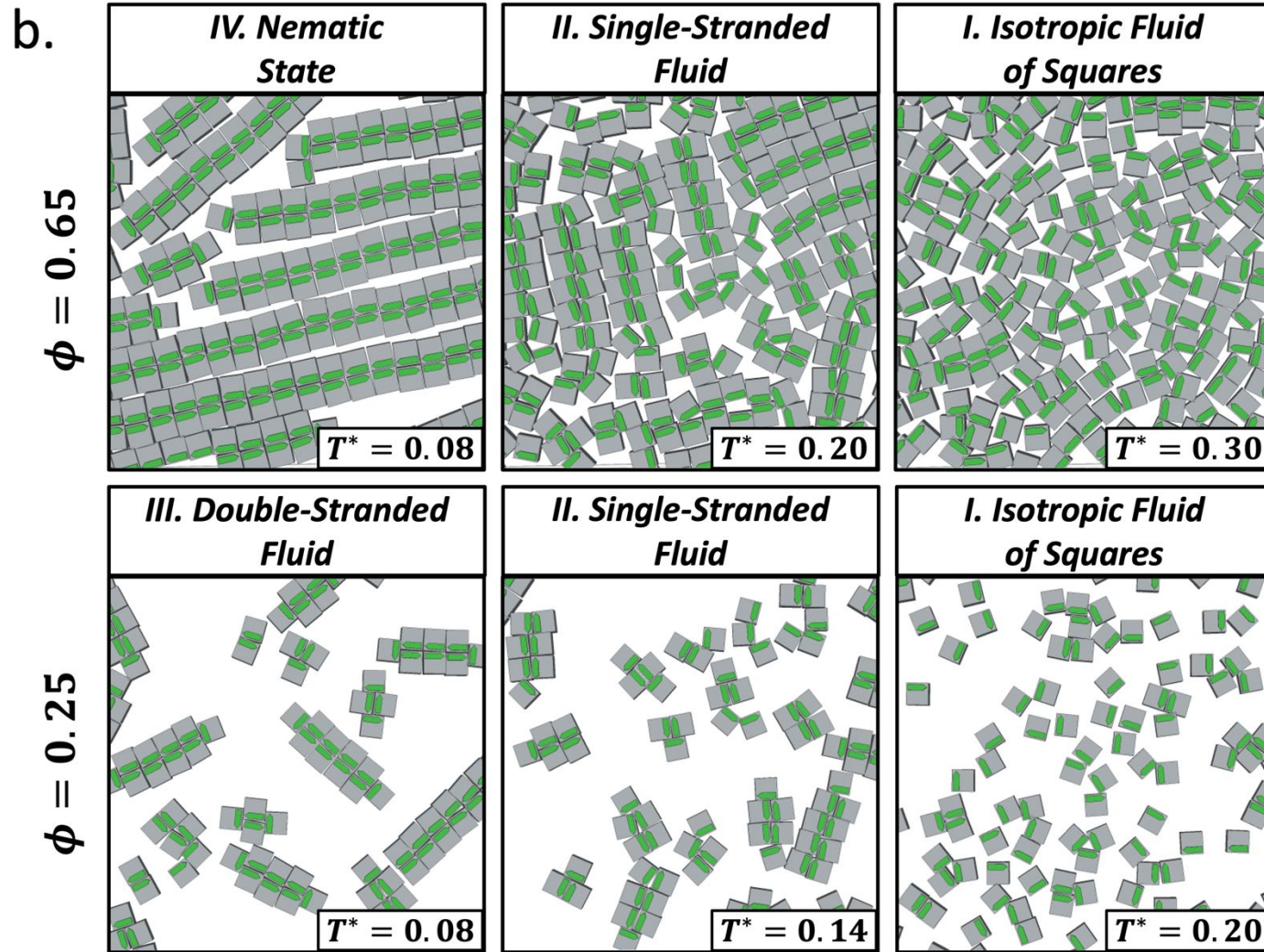


Fig. 6 (a) Phase diagram in the area fraction vs. reduced temperature plane for single-chirality systems of squares with standard dipoles. In the phase diagram, the dotted line represents the system's density threshold required for the system to form a nematic state. Below the dashed line the system will not form a nematic state while above the dashed line the system sometimes forms a nematic state. (b) Simulation snapshots show structural properties of single-chirality systems of squares with standard dipoles at various densities and temperatures. In each snapshot, squares are gray; the A-chirality squares have dipoles shown as green arrows.





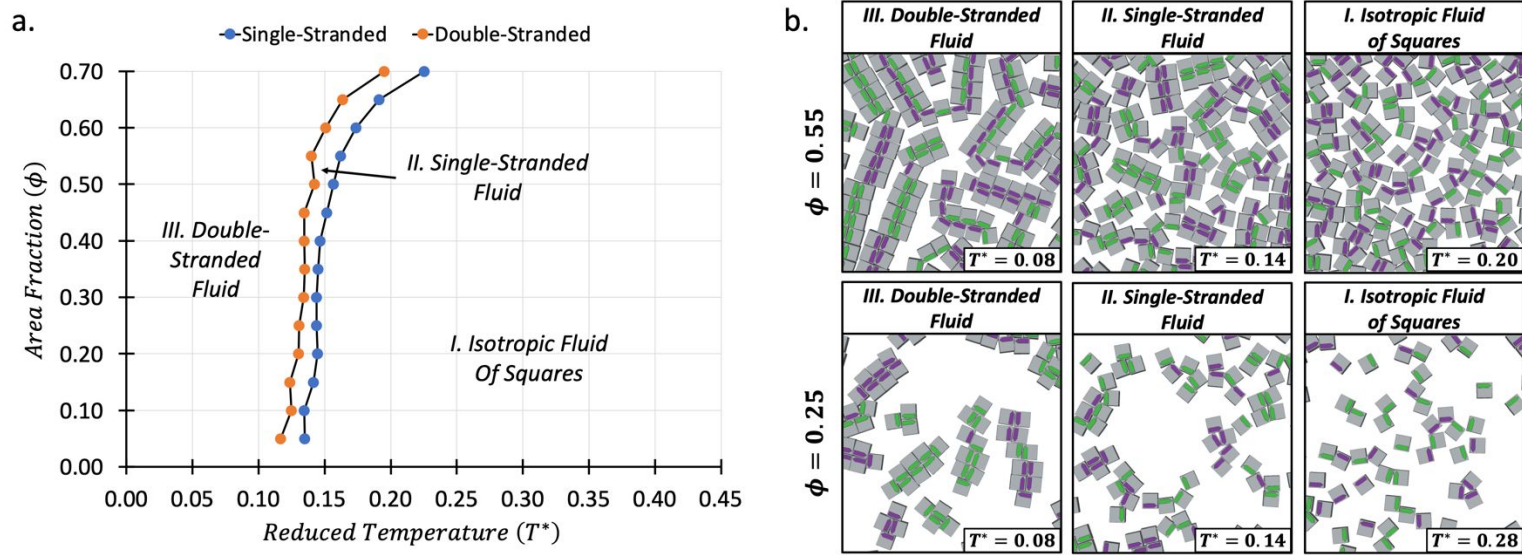


Fig. 7 (a) Phase diagram in the area fraction vs. reduced temperature plane for mixed-chirality systems of squares with standard dipoles. (b) Simulation snapshots show structural properties of mixed-chirality systems of squares with standard dipoles at various temperatures and densities. In each snapshot, squares are gray, where A-chirality squares have dipoles shown as green arrows and B-chirality squares have dipoles shown as purple arrows.

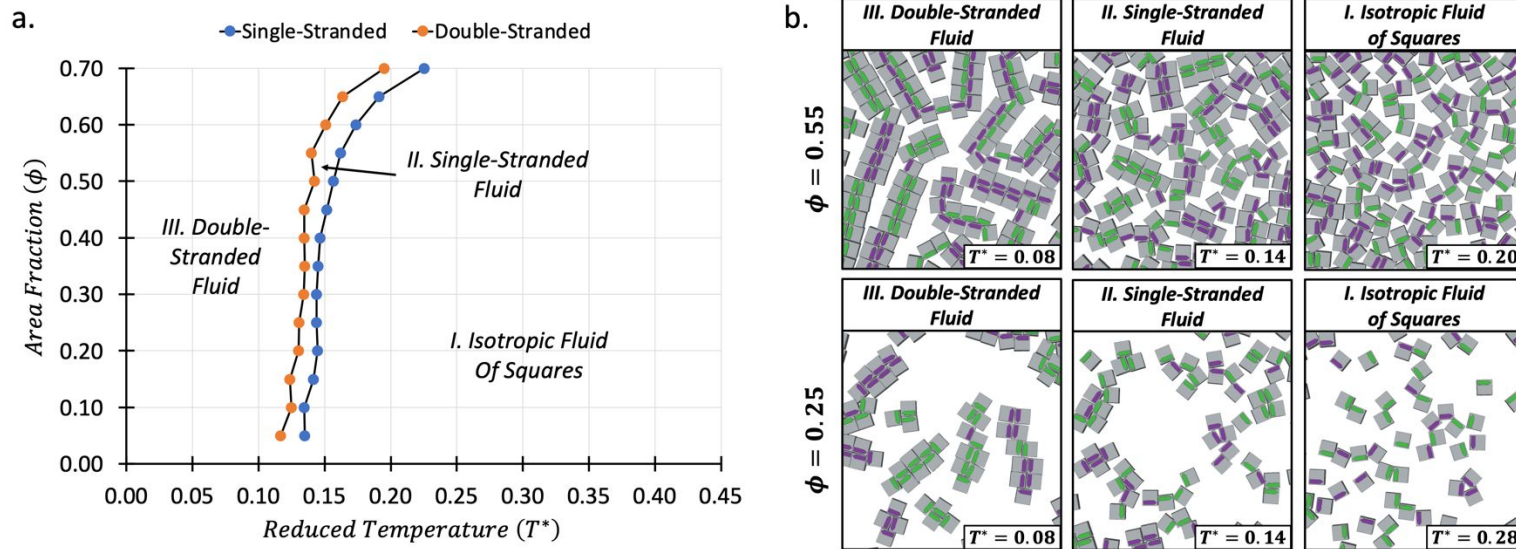
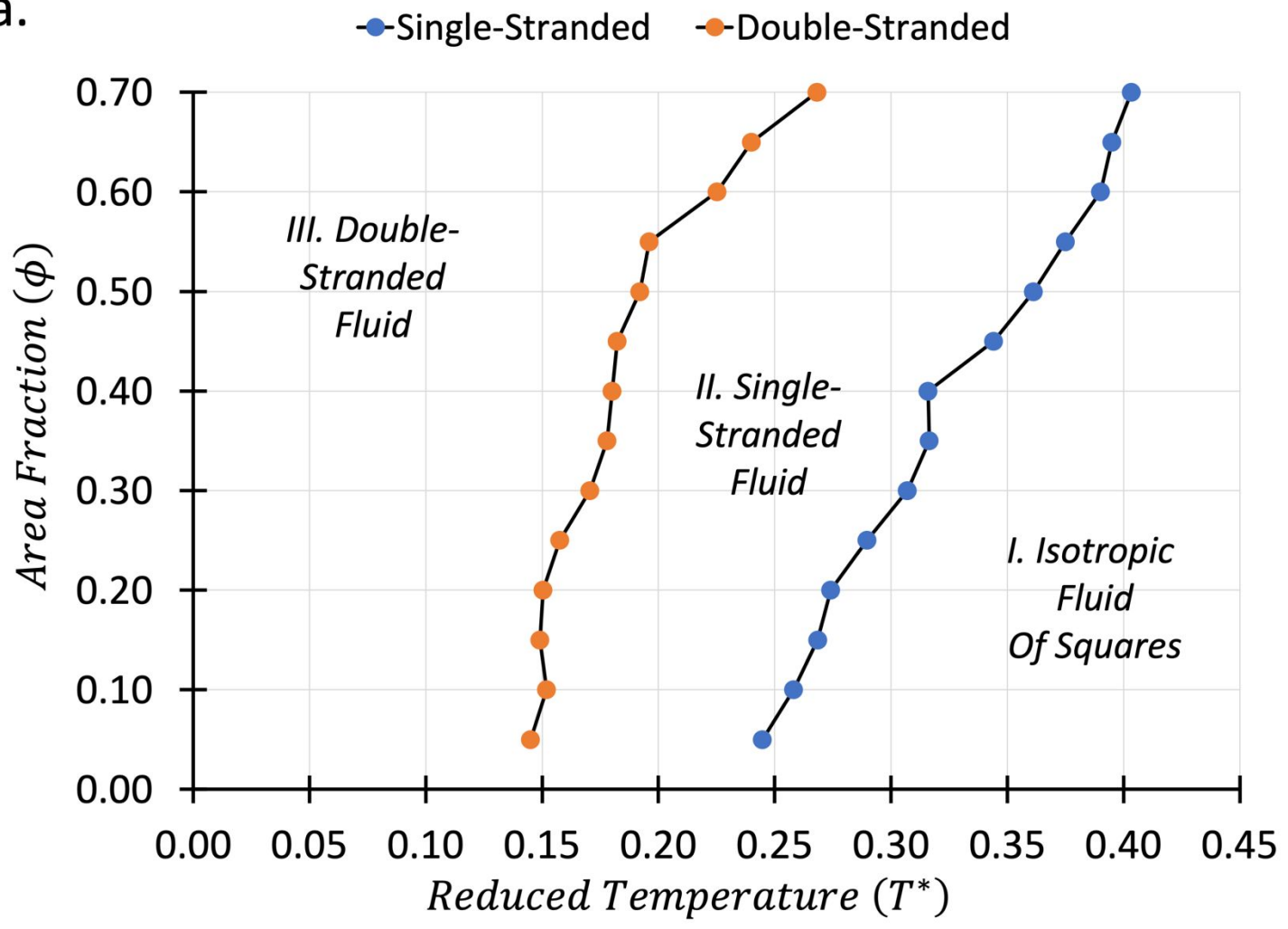
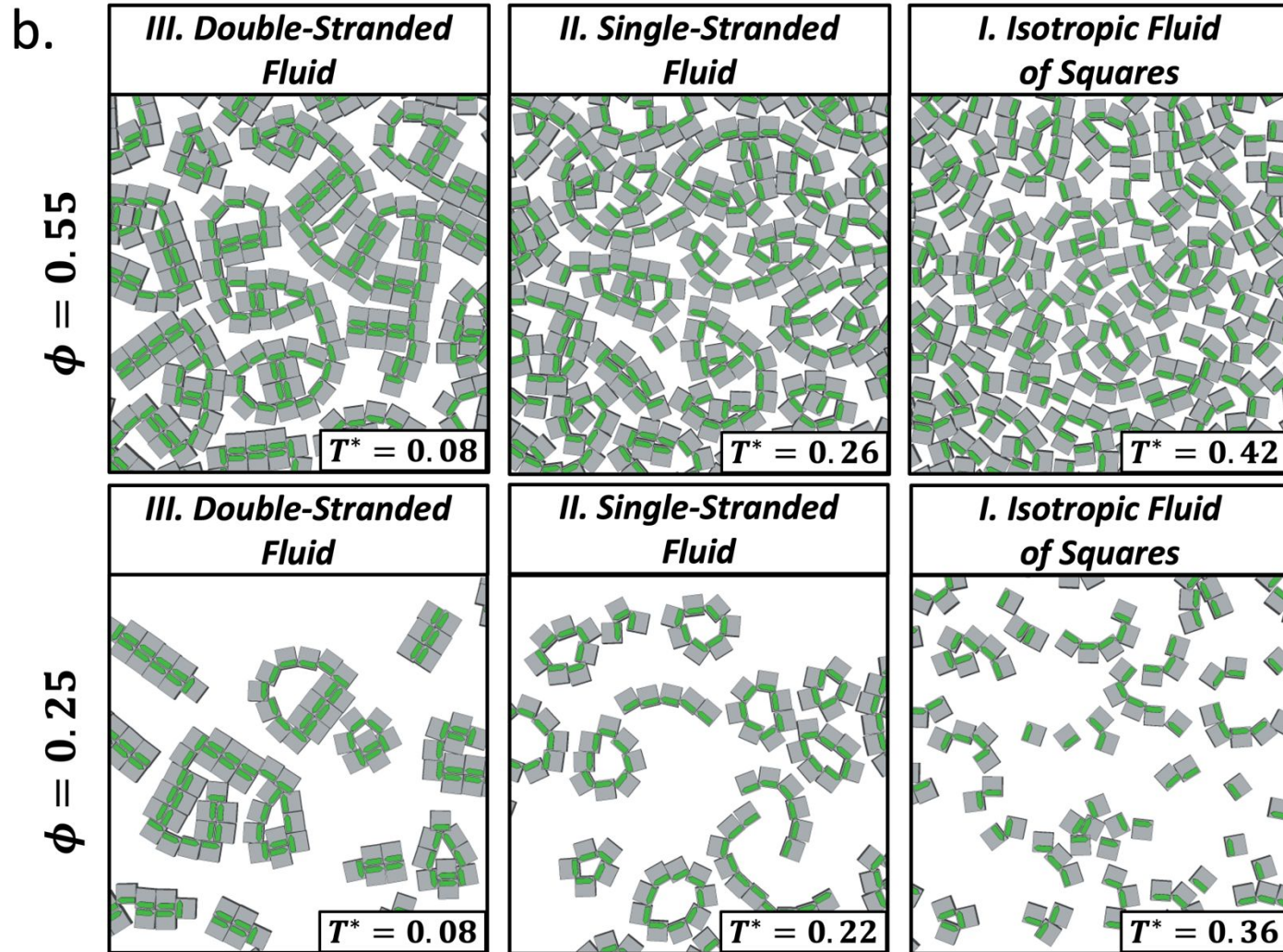


Fig. 7 (a) Phase diagram in the area fraction vs. reduced temperature plane for mixed-chirality systems of squares with standard dipoles. (b) Simulation snapshots show structural properties of mixed-chirality systems of squares with standard dipoles at various temperatures and densities. In each snapshot, squares are gray, where A-chirality squares have dipoles shown as green arrows and B-chirality squares have dipoles shown as purple arrows.

a.





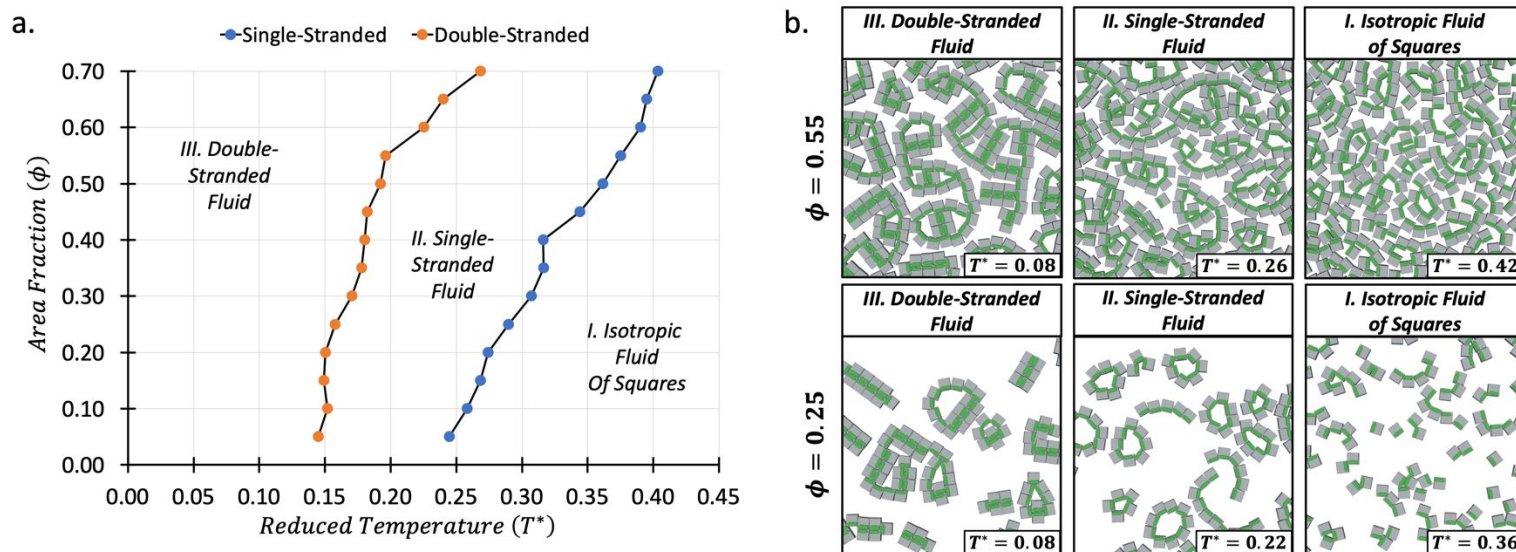


Fig. 8 (a) Phase diagram in the area fraction vs. reduced temperature plane for single-chirality systems of squares with offset dipoles. (b) Simulation snapshots show structural properties of single-chirality systems of squares with offset dipoles at various temperatures and densities. In each snapshot, squares are gray; the A-chirality squares have dipoles shown as green arrows.

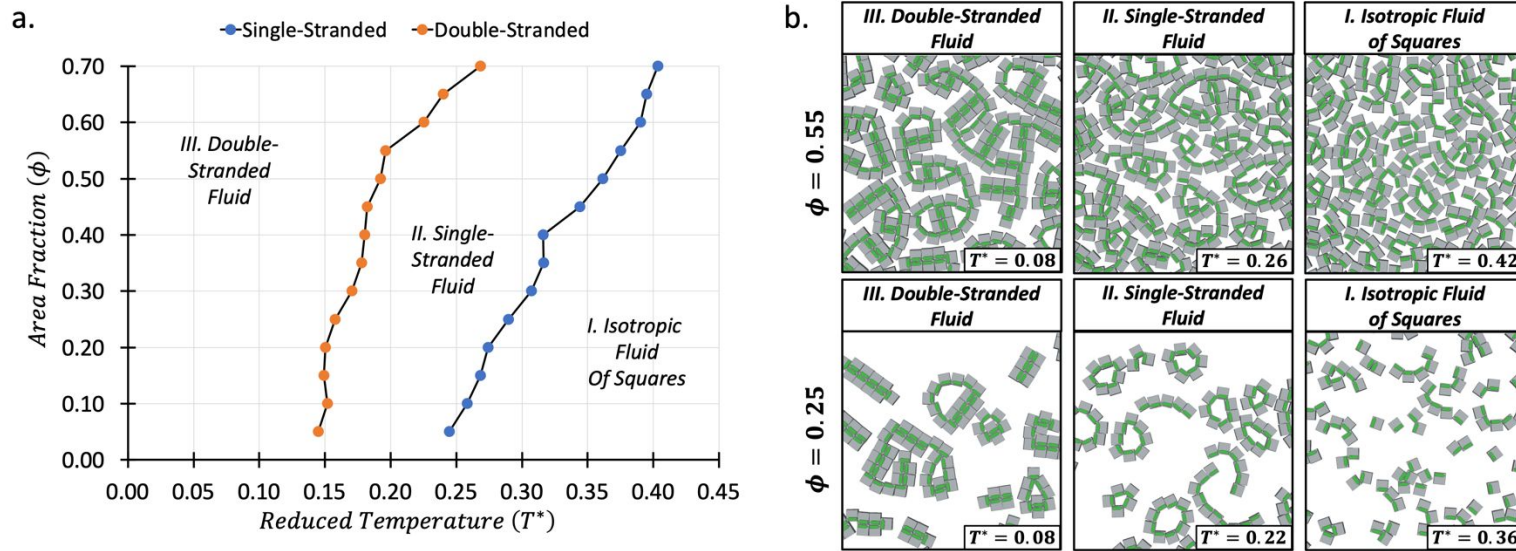
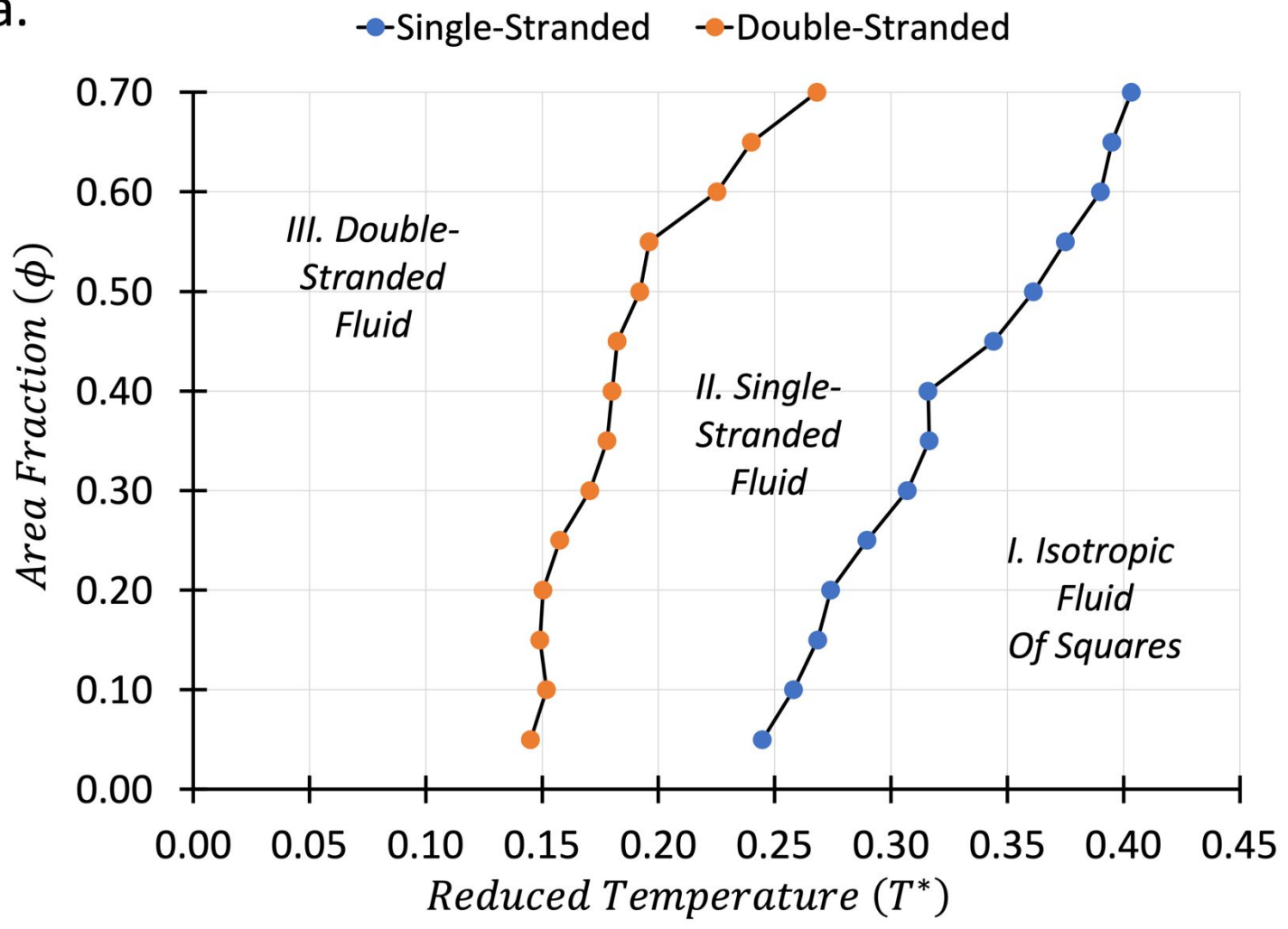
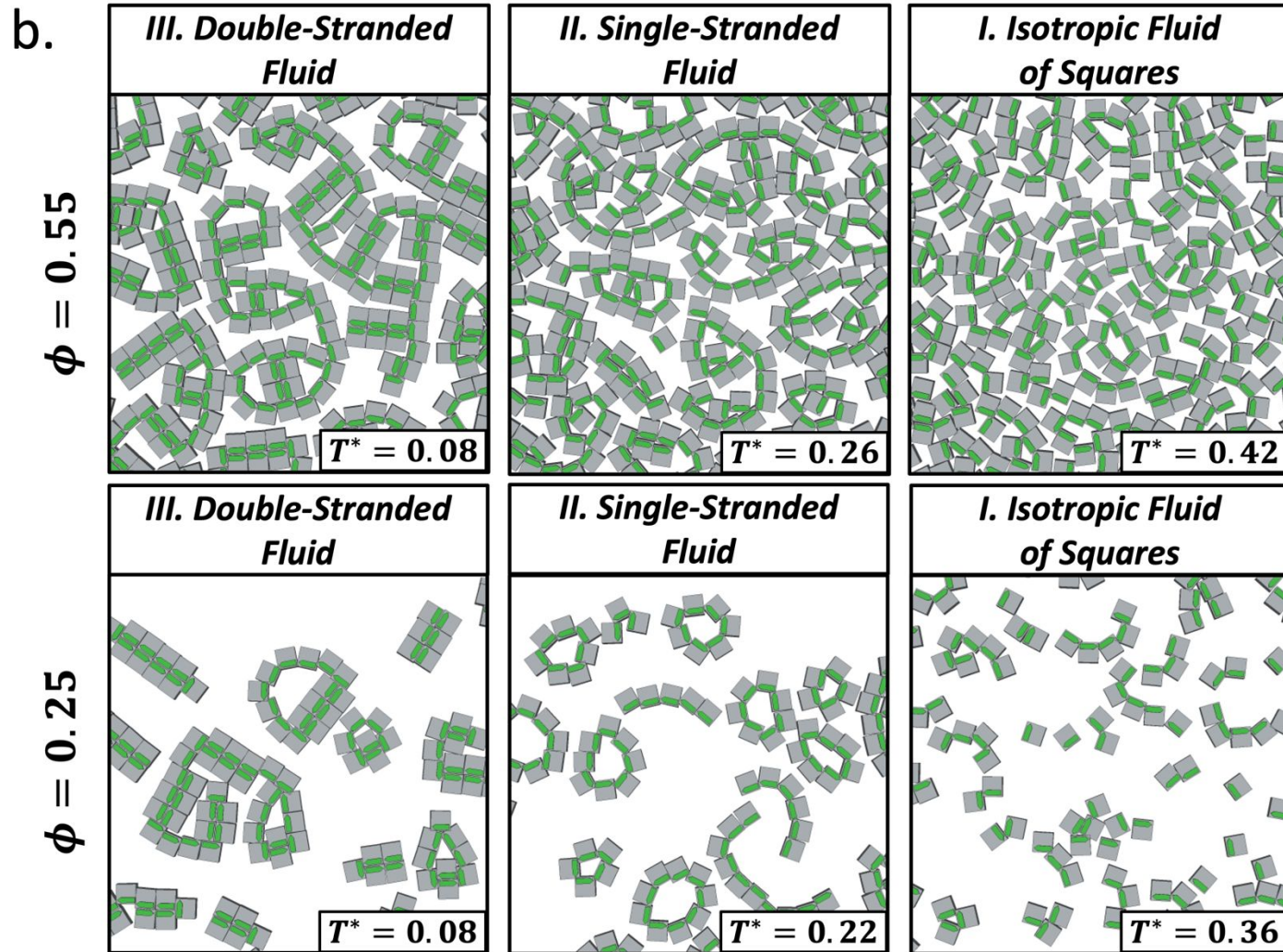


Fig. 8 (a) Phase diagram in the area fraction vs. reduced temperature plane for single-chirality systems of squares with offset dipoles. (b) Simulation snapshots show structural properties of single-chirality systems of squares with offset dipoles at various temperatures and densities. In each snapshot, squares are gray; the A-chirality squares have dipoles shown as green arrows.

a.





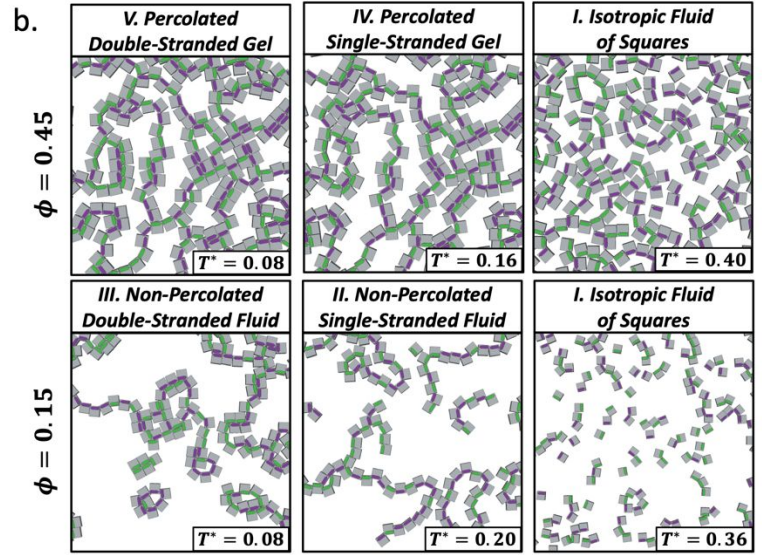
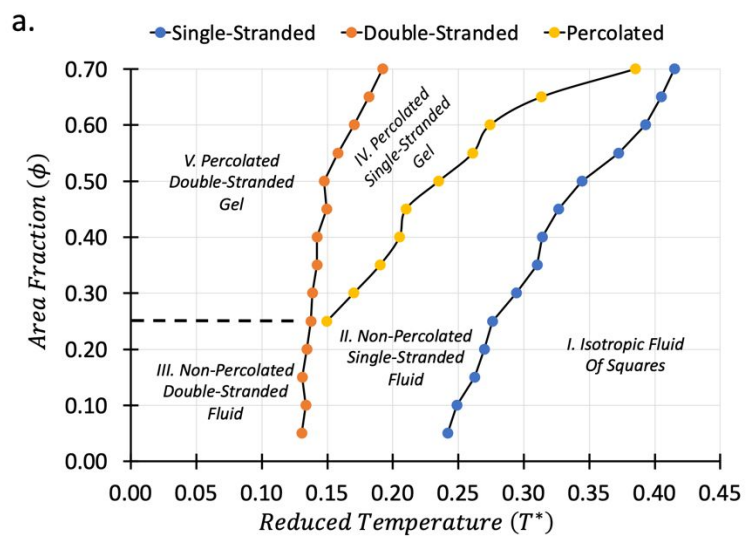


Fig. 9 (a) Phase diagram in the area fraction vs. reduced temperature plane for mixed-chirality systems of squares with offset dipoles. In the phase diagram, the dashed line represents the system’s density threshold required for the system to form a percolated state. Below the dashed line the system will not form a percolated state; above it the system forms a percolated state. (b) Simulation snapshots show structural properties of mixed-chirality systems of squares with offset dipoles at various temperatures and densities. In each snapshot, squares are gray; A-chirality squares have dipoles shown as green arrows and B-chirality squares have dipoles shown as purple arrows.

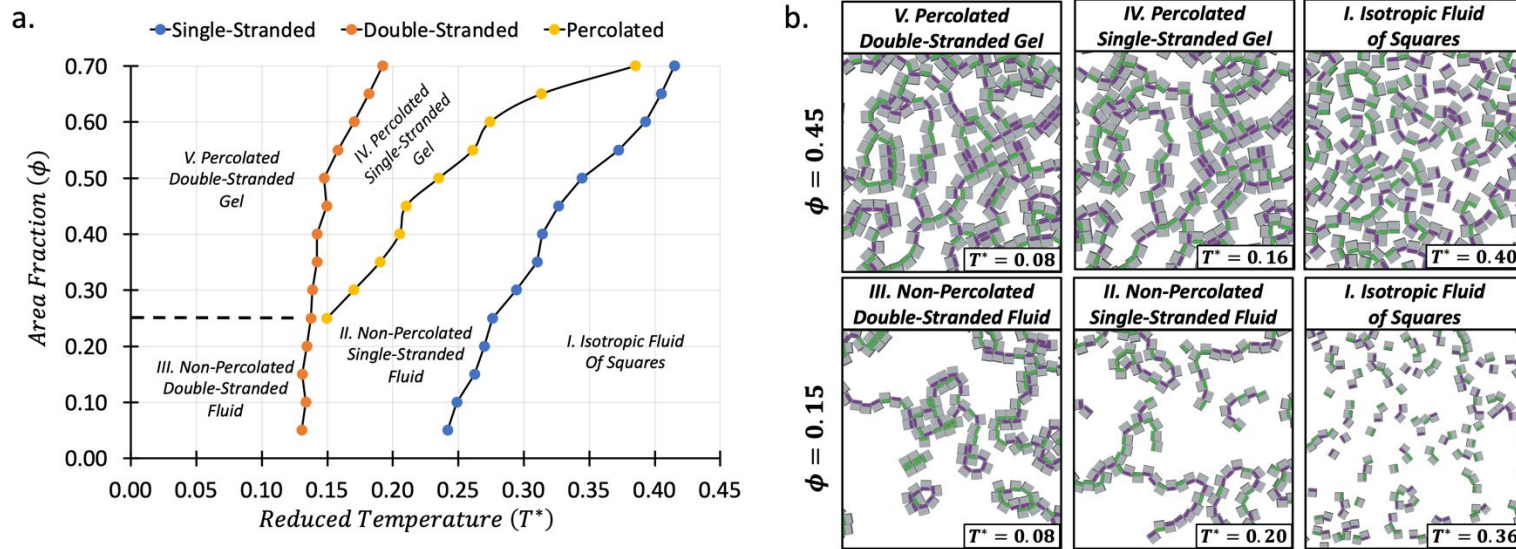


Fig. 9 (a) Phase diagram in the area fraction vs. reduced temperature plane for mixed-chirality systems of squares with offset dipoles. In the phase diagram, the dashed line represents the system's density threshold required for the system to form a percolated state. Below the dashed line the system will not form a percolated state; above it the system forms a percolated state. (b) Simulation snapshots show structural properties of mixed-chirality systems of squares with offset dipoles at various temperatures and densities. In each snapshot, squares are gray; A-chirality squares have dipoles shown as green arrows and B-chirality squares have dipoles shown as purple arrows.

